Molecular Insights into New Particle Formation in Barcelona, Spain

**James Brean[1], David C.S. Beddows[1], Zongbo Shi[1],
Brice Temime-Roussel[2], Nicolas Marchand[2], Xavier Querol[3],
Andrés Alastuey[3], María Cruz Minguillón[3], and
Roy M. Harrison[1a*]**

**[1]Division of Environmental Health and Risk Management
School of Geography, Earth and Environmental Sciences
University of Birmingham, Edgbaston, Birmingham B15 2TT
United Kingdom**

**[2]Aix Marseille Univ, CNRS, LCE
Marseille, 13003, France**

**[3]Institute of Environmental Assessment and
Water Research (IDAEA-CSIC), Barcelona, 08034 Spain**

[a]Also at: Department of Environmental Sciences / Center of Excellence in Environmental Studies, King Abdulaziz University, PO Box 80203, Jeddah, 21589, Saudi Arabia

---

[*] To whom correspondence should be addressed (Email: r.m.harrison@bham.ac.uk)

ABSTRACT

Atmospheric aerosols contribute some of the greatest uncertainties to estimates of global radiative forcing, and have significant effects on human health. New particle formation (NPF) is the process by which new aerosols of sub-2 nm diameter form from gas-phase precursors and contributes significantly to particle numbers in the atmosphere, accounting for approximately 50% of cloud condensation nuclei globally. Here, we study summertime NPF in urban Barcelona in NE Spain utilising particle counting instruments down to 1.9 nm and a Nitrate CI-APi-ToF. The rate of formation of new particles is seen to increase linearly with sulphuric acid concentration, although particle formation rates fall short of chamber studies of H_2SO_4-DMA-H_2O, while exceeding those of H_2SO_4-BioOxOrg-H_2O nucleation, although a role of highly oxygenated molecules (HOMs) cannot be ruled out. The sulphuric acid dimer:monomer ratio is significantly lower than that seen in experiments involving sulphuric acid and DMA in chambers, indicating that stabilization of sulphuric acid clusters by bases is weaker in this dataset than in chambers, either due to rapid evaporation due to high summertime temperatures, or limited pools of stabilising amines. Such a mechanism cannot be verified in this data, as no higher-order H_2SO_4-amine clusters, nor H_2SO_4-HOM clusters were measured. The high concentrations of HOMs arise from isoprene, alkylbenzene, monoterpene and PAH oxidation, with alkylbenzenes providing greater concentrations of HOMs due to significant local sources. The concentration of these HOMs shows a dependence on temperature. The organic compounds measured primarily fall into the SVOC volatility class arising from alkylbenzene and isoprene oxidation. LVOC largely arise from oxidation of alkylbenzenes, PAHs and monoterpenes, whereas ELVOC arise from primarily PAH and monoterpene oxidation. New particle formation without growth past 10 nm is also observed, and on these days oxygenated organic concentrations are lower than on days with growth by a factor of 1.6, and thus high concentrations of low volatility oxygenated organics which primarily derive from traffic-emitted VOCs appear to be a necessary condition for the growth of newly formed particles in Barcelona. These results are consistent with prior observations of new particle formation from sulphuric acid-

amine reactions in both chambers and the real atmosphere, and are likely representative of the urban background of many European Mediterranean cities. A role for HOMs in the nucleation process cannot be confirmed or ruled out, and there is strong circumstantial evidence for the participation of HOMs across multiple volatility classes in particle growth.

1. INTRODUCTION

Atmospheric aerosols, defined as liquid or solid droplets suspended in a gas, affect the climate both directly by scattering and absorbing radiation, and indirectly by acting as cloud condensation nuclei (CCN) (Penner et al., 2011), providing great uncertainties in estimates of global radiative forcing (IPCC, 2014). Further, fine ambient aerosols (defined as those with diameter below 2.5 μm) are the fifth greatest global mortality risk factor, resulting in 103.1 million disability-adjusted life year loss in 2015 (Cohen et al., 2017). The number concentration of the ultrafine fraction of these (aerosols with diameter below 0.1 μm, referred to as ultrafine particles or UFP) pose potentially significant health risks also, due to their high concentration and surface area. The more diffuse, gas-like behaviour of UFP allows them to penetrate into the deep lung and enter the bloodstream (Miller et al., 2017). Ultrafine particles occur in the urban environment either as primary emissions (e.g., from car exhaust (Harrison et al., 2018)) or secondarily as the product of new particle formation (NPF) (Brines et al., 2015; Guo et al., 2014; Kulmala et al., 2017; Lee et al,. 2019)

NPF is the formation of aerosol particles from gas-phase precursors. NPF can be considered a two-step process involving initial formation of a cluster of gas molecules at the critical diameter at around 1.5 nm - the diameter at which a free-energy barrier must be overcome to allow the spontaneous phase transition from gas to liquid or solid (Zhang et al., 2012), and the subsequent growth of this droplet to a larger aerosol particle. The first step of this process is dependent upon the stability and abundance of the clustering molecules. Sulphuric acid, water, and dimethylamine (DMA), for example, efficiently form particles as the strong hydrogen bonding between the acid base pair produces near negligible evaporation, much lower than the evaporation rate seen for the more weakly bound sulphuric acid-ammonia-water system. Nucleation of sulphuric acid, DMA and water proceeds at, or near to the kinetic limit in a chamber at 278 K when DMA mixing ratios are sufficient (Almeida et al., 2013; Kürten et al., 2014). Once past this 1.5 nm diameter, condensation and coagulation will drive particle growth. Both the abundance of condensable gases and their vapour pressures limit condensational growth. Vapour pressures are especially important for the initial growth stages, as the Kelvin effect barrier impairs condensation of more volatile species, with this condition of low vapour pressures becoming less significant as the diameter of the particle increases (Tröstl et al., 2016). Once sufficiently large (>50 nm), the loss processes of coagulation and evaporation of these particles become inefficient, resulting in a significant atmospheric lifetime. It is from these these diameters onwards the climate forcing effects of these particles become most pronounced.

NPF processes happen globally, across a diverse range of environments from pristine polar regions, to polluted urban megacities (Kerminen et al., 2018), and represent a significant source of CCN, with 10-60% of NPF events shown to produce CCN and enhancement factors to CCN count ranging from 0.5 – 11 (Lee et al., 2019 and references within). Strong NPF events are observed across a range of urban environments, despite high condensation sinks $>10^{-2}$ s^{-1} (Bousiotis et al., 2019; Yu et al., 2016), and can act as a precursor to strong haze events (Guo et al., 2014). The occurrence of urban NPF has only been partially explained by growing understanding from recent in-depth studies (Yao et al., 2018). Recent advances in instrumentation allow for the measurement of particles down to the critical diameter with instruments such as the particle size magnifier (PSM), and (Neutral) Air Ion Spectrometer (NAIS/AIS) (Lee et al., 2019), and mass spectral techniques for measuring the abundance and composition of neutral (Jokinen et al., 2012) and charged (Junninen et al., 2010) clusters. Elucidated mechanisms with these techniques involve sulphuric acid and ammonia in remote environments (Jokinen et al., 2018; Yan, 2018), monoterpene derived highly oxygenated molecules (HOM) in remote environments (Rose et al., 2018), iodic acid in coastal environments (Sipilä et al., 2016), and sulphuric acid and DMA in polluted urban environments (Yao et al., 2018).

Urban Barcelona sees frequent, strong summer-time NPF events occurring on 28% of days. These events are associated with high insolation and elevated ozone (~60 $\mu g\ m^{-3}$) when considering the whole year (Brines et al., 2014, 2015).Ground-level observations report NPF events starting typically at midday, and either occurring in urban Barcelona and the surrounding regional background simultaneously, or isolated to eitherurban Barcelona or just the regional background (Dall'Osto et al., 2013). Vertical profiles over urban Barcelona reveal that NPF occurs at higher altitudes, and starts earlier in the day, as at a given altitude these events are not suppressed by early traffic peaks contributing to particle load (Minguillón et al., 2015). Here, we examine gas phase mass spectral evidence and particle formation rates at the critical diameter from sulphuric acid in Barcelona, with possible contribution from strong bases and highly oxygenated organic molecules (HOMs), as well as factors influencing subsequent particle growth.

2. METHODS

2.1 Sampling Site

The Palau Reial site in Barcelona (41°23'15" N, 2°6'53.64" E) is representative of the urban background of Barcelona, located at the Institute of Environmental Assessment and Water Research (IDAEA-CSIC) in the north-west of the city. Sampling was performed from a container 20 m from a low traffic road, and 200 m from the nearest main road (Avinguda Diagonal). Data were taken from 2018/06/28 through 2018/07/18.

2.2 Chemical Ionisation Atmospheric Pressure Interface Time of Flight Mass Spectrometry

The Aerodyne Nitrate Chemical Ionisation Atmospheric Pressure interface Time of Flight Mass Spectrometer (CI-APi-ToF) was used to make measurements of neutral oxygenated organic compounds, organic and inorganic acids, bases, and their molecular clusters at high time resolution with high resolving power. The ionization system charges molecules by adduct formation, such as in the case of organic compounds with two or more hydrogen bond donor groups (Hyttinen et al., 2015), or proton transfer in the case of strong acids like sulphuric acid (Jokinen et al., 2012).

Hydroxyl or hydroperoxyl functionalities are both common hydrogen bond donating groups, with hydroperoxyl being the more efficient hydrogen bond donor (Møller et al., 2017). This instrument has been explained in great detail elsewhere (Jokinen et al., 2012; Junninen et al., 2010), but briefly, the front end consists of a chemical ionisation system where a 10 L min^{-1} sample flow is drawn in through the 1 m length 1" OD stainless steel tubing opening. A secondary flow was run parallel and concentric to this sample flow, rendering the reaction chamber effectively wall-less. A 3 cm^3 min^{-1} flow of a carrier gas (N_2) is passed over a reservoir of liquid HNO_3, entraining vapour which is subsequently ionised to NO_3^- via an X-ray source. Ions are then guided into the sample flow. The nitrate ions will then charge molecules either by clustering or proton transfer. The mixed flows travelling at 10 L min^{-1} enter the critical orifice at the front end of the instrument at 0.8 L min^{-1} and are guided through a series of differentially pumped chambers before reaching the ToF analyser. All data analysis was carried out in the Tofware package in Igor Pro 7 (Tofwerk AG, Switzerland). Signals except for those of amines and ammonia are divided by the sum of reagent ion signals and multiplied by a calibration coefficient to produce a concentration. A calibration coefficient of 3×10^9 cm^{-3} was established based upon comparison with a sulphuric acid proxy (Mikkonen et al., 2011) and is in line with a prior calibration with our instrument (Brean et al., 2019). Uniform sensitivity between H_2SO_4 and all other species measured by CI-APi-ToF bar amines and ammonia was assumed in this work. This introduces some uncertainties, as it relies upon both collision rates and charging efficiencies to be the same within the ionisation source for all species. Amine and ammonia signals are normalised to the nitrate trimer signal (Simon et al., 2016). Prior reports of ammonia and amines as measured by CI-APi-ToF employed corona discharge systems, which utilise higher concentrations of nitric acid, thus we report normalised signals. We present correlations of each of these bases clustered with the nitrate dimer plotted against measurements with the nitrate trimer, as well as their intercorrelations and example peak fits across Figure S1. C_2 amines, C_4 amines and ammonia were the only molecules of this kind found in our mass spectra. Systematic uncertainties of +100% / -50 % arising from this method are assumed.

Due to the high resolving power of the CI-APi-ToF system (mass resolving power of 3000, and mass accuracy of 20 ppm at 201 m/Q), multiple peaks can be fit at the same unit mass and their molecular formulae assigned. Beyond 500 m/Q, peak fitting and assignment of compositions becomes problematic as signal decreases, mass accuracy decreases, and the total number of possible chemical compositions increases, so peaks above the C_{20} region have not been assigned (Cubison and Jimenez, 2015), however, signals past this region tended to be extremely low. All ions identified are listed in Table S1. As proton transfer mostly happens with acids, and nearly all HOM molecules will be charged by adduct formation it is possible to infer the uncharged formula; therefore, all HOMs from here onwards will be listed as their uncharged form. The CI-APi-ToF inlet was placed approximately 1.5 m a.g.l. CI-APi-ToF data is only available between the dates 2018/07/06 and 2018/07/17.

2.2 Particle Size and Number Measurements

Two Scanning Mobility Particle Sizer (SMPS) instruments measured particle size distributions at 5 minute time resolution, one Long Column SMPS (TSI 3080 EC, 3082 Long DMA, 3772 CPC, TSI, USA) and one NanoSMPS (3082 EC, 3082 Nano DMA, 3776 CPC, TSI, USA) measuring the ranges 10.9 – 478.3 nm and 4.5 – 65.3 nm respectively. A Particle Size Magnifier (A10, Airmodus, FN) linked to a CPC (3775, TSI, USA) measured the sub-3 nm size fraction. The PSM was run in stepping mode, operating at four different saturator flows to vary the lower size cut of particles that it will grow (defined as the point of 50% efficiency, D_{50}). The instrument provided D_{50} from 1.4 to 2.4 nm. The instrument switched between saturator flows each 2.5 minutes, giving a sub-2.4 nm size distribution every 10 minutes. Aerosol sampling inlets were placed approximately 2 m a.g.l.

2.3 Other Measurements

Mixing ratios of non-methane VOC with proton affinity greater than H_3O^+ were made using the proton transfer reaction time of flight mass spectrometer (PTR-ToF-MS 8000, Ionicon Analytik

GmbH, Austria). A detailed description of the instrument is provided by Graus et al., (2010) The sampling set up, operating conditions, and quantification procedures are similar to those described in Minguillón et al. (2016). Continual monitoring of composition and mass of submicron aerosol >75 nm was carried out with an Aerosol Chemical Speciation Monitor (ACSM, Aerodyne, USA) (Ng et al., 2011). Ozone, NO, and NO_2 were measured by conventional ultraviolet and chemiluminiscence air quality instrumentation. Meteorological data were supplied by the Faculty of Physics of University of Barcelona, from a nearby (200 m from the measurement site) meteorological station located at the roof of an 8 floor building.

2.4 Condensation Sink and Particle Growth Rate

The condensation sink (CS) represents the rate at which a vapour phase molecule will collide with pre-existing particle surface, and was calculated from the size distribution data as follows (Kulmala et al., 2012):

$$CS = 4\pi D \ \sum_{d_p} \beta_{m,d_p} d_p N_{d_p} \ , \tag{1}$$

where D is the diffusion coefficient of the diffusing vapour (assumed sulphuric acid), β_m is a transition regime correction (Kulmala et al., 2001), d_p is particle diameter, and N_{dp} is the number of particles at diameter d_p. The formation rate of new particles at size d_p is calculated as follows:

$$J_{d_p} = \frac{dN_{d_p}}{dt} + \ CoagS_{d_p} \, .N_{d_p} + \frac{GR}{\Delta d_p} . N_{d_p} \tag{2}$$

where the first term on the right-hand side comprises the rate at which particles enter the size d_p, and the latter two terms represent losses from this size by coagulation and growth respectively. J_5 was calculated using the data between 5 - 10 nm, and $J_{1.9}$ was calculated using the measurements between 1.9 – 4.5 nm. We also calculated $J_{1.9}$ from our NanoSMPS data, employing the equations of Lehtinen et al. (2007). $J_{1.9}$ from both methods showed reasonable agreement ($R^2 = 0.34$). Agreement between J_5 and $J_{1.9}$ for each method was similar ($R^2 = 0.37$ and $R^2 = 0.38$ for $J_{1.9}$ calculated from PSM data and from Lehtinen et al. (2019) respectively). $J_{1.9}$ is greater than J_5 as predicted from equation (2) by around a factor of 20. See Kulmala et al. (2001) for more information on calculation of coagulation sinks and formation rates. Growth rates between 4.5 – 20 nm were calculated according to the lognormal distribution function method (Kulmala et al., 2012), whereas those between 1.9 and 4.5 nm were calculated from PSM data using a time-delay method between PSM and NanoSMPS data. Systematic uncertainties on our calculated $J_{1.9}$ values include 25% method uncertainty (Yli-Juuti et al., 2017), with a further 25% arising from uncertainties in PSM cutoff (± 0.5 nm), as well as a 10% uncertainty in counting errors. A 50% error arising from calculated coagulation sink is also applied (Kurten et al., 2016). The above calculations rely on the assumption of homogeneous air masses, and while air mass advection, as well as primary particle emissions can cause errors in estimations of temporal changes in particle count and diameter, the appearance and persistence of a new mode of particles across a period of several hours is typically indicative of a regional process.

Growth rates from irreversible condensation of various vapours were calculated as according to Nieminen et al. (2010). At our measured relative humidity, sulphuric acid favours binding to 2 H_2O molecules (Kúrten et al., 2007). As amine concentrations are likely limited, we presume no mass from amines in the condensing species. H_2SO_4 was assigned a density of 1.8 g cm^{-3}. For simplicity, the properties of MSA regarding density and hydration were presumed the same as H_2SO_4, and HIO_3 was presumed to have the same hydration as H_2SO_4, with a density of 4.98 g cm^{-3}. The density of condensing organic vapours was assumed 1.5 g cm^{-3}, and concentration-weighted mean mass (~276 g mol^{-1} for LVOC) and atomic weighted diffusion volumes of organic compounds were used to calculate GRs.

2.4 DBE and 2D-VBS

The double bond equivalent (DBE) describes the degree of unsaturation of an organic molecule and is defined simply as:

$$DBE = N_C - \frac{N_H}{2} - \frac{N_N}{2} + 1 \qquad (3)$$

The saturation vapour pressure at 300 K is defined by the 2D-volatility basis set (2D-VBS) as follows, if all nitrogen functionality is assumed to take the form -ONO_2 (Bianchi 2019; Donahue 2011; Schervish and Donahue, 2020):

$$Log_{10}(C^*)(300\ K) = (N_{C0} - N_C)b_C - N_O b_O - 2\frac{N_O N_C}{N_C + N_O} b_{CO} - N_n b_N \qquad (4)$$

where N_C, N_H, and N_N, are the number of carbon, hydrogen, and nitrogen atoms respectively. N_O is the number of oxygen atoms minus $3N_N$ to account for -ONO_2 groups, N_{C0} is 25 (the carbon number of a 1 µg m^{-3} alkane), b_C, b_O, b_{CO}, and b_N are 0.475, 0.2, 0.9 and 2.5 respectively, and represent interaction and nonideality terms. The final term of equation (4) represents the -ONO_2 groups, each reducing the saturation vapour pressure by 2.5 orders of magnitude. C^* values are calculated at 300 K and not corrected for temperature, as 300 K is within 1 K of the campaign average temperature.

3. RESULTS AND DISCUSSION

3.1 General Conditions of NPF Events

Summer NPF events in the regional background around Barcelona are associated with high insolation, relatively low ozone (high compared with the rest of the year), and lower particulate matter load (Brines et al., 2014; Carnerero et al., 2019). Figure 1 shows an example of a day with no NPF in panel (a), referred to as "non-event" here, where two traffic-associated peaks in particle number are seen during rush hours. Midday traffic peaks are also seen on certain days, but these are easily distinguished from nucleation processes due to the lack of a significant <10 nm mode. Figure 1(b) shows a nucleation day with growth to larger sizes >10 nm, termed “full-event”, showing the growth through the course of the day. These fulfil all the criteria of Dal Maso et al. (2005). 4 events of this type were observed with CI-APi-ToF data coverage. Figure 1(c) shows a day with nucleation occurring, but no growth past 10 nm. These days are referred to as “burst-event” days. Here, NPF is seen to occur, but particles fail to grow past the nucleation mode. 2 such events were seen in this data with CI-APi-ToF data coverage, and both are accompanied by a distinct mode appearing beforehand at ~20-40 nm. Condensation sinks were not significantly higher than on full event days, so this failure of particles to grow further cannot be attributed to condensational (or coagulational) losses. $GR_{4.5\text{-}20}$ ranged between 2.47 – 7.31 nm h^{-1} (4.69 ± 2.03 nm h^{-1}), $GR_{1.9\text{-}4.5}$ ranged between 3.12 – 5.20 nm h^{-1} (4.36 ± 1.02 nm h^{-1}). The survival parameter (P) as suggested by Kulmala et al. (2017) is defined as $CS \cdot 10^{-4} / GR$, and for this data is equal to 82, higher than other European cities. The occurrence of such a high P value should, in theory, inhibit the occurrence of NPF, but we show events happen readily under such conditions, akin to other heavily polluted megacities.

Figure 2 contains box plots showing condensation sink, temperature and global radiation for all 3 NPF types across the entire day (diurnal profiles plotted in Figure S2). Condensation sinks during NPF periods of both types (Figures 1(b) & 1(c)) were not significantly lower than in non-event periods. Condensation sinks were supressed prior to the beginning of an event for full-events, increasing relative to non-events through the afternoon period. Of the two burst-events, one was similarly characterised by a suppression to condensation sink, whereas the other showed a sharp rise in the midday. Global radiation and temperature were higher for full-events, most significantly for temperature. Figure 3 is as Figure 2 but for sulphuric acid, ammonia and amines, and HOMs as measured by CI-APi-ToF (HOM criteria are discussed in section 3.3.1). Sulphuric acid is elevated during both full-event and burst-event periods. In urban Barcelona, sulphuric acid will primarily arise from oxidation of SO_2 by the $OH^·$ radical, with anthropogenic emissions such as shipping emissions from the port areas being significant sources of SO_2 (Henschel et al., 2013). Direct traffic emissions have been shown to be a significant primary sulphuric acid source (Olin et al., 2020), but our sulphuric acid data show no traffic peaks. Ammonia and amines show enhancement for full-event periods, but not burst-event periods. Nucleation rates (at typical tropospheric sulphuric acid concentrations) are sensitive to amine concentrations in the range of a few pptv, with enhancements to amine mixing ratios past this point increasing the nucleation rate marginally (Almeida et al., 2013), while typical concentrations of DMA and other alkylamines vary from zero to a few pptv in the boundary layer (Ge et al., 2011a).

Barcelona has been shown to contain ppbv levels of ammonia (Pandolfi et al., 2012), arising from both agriculture to the north (Van Damme et al., 2018), and anthropogenic activities such as waste management and traffic, with waste management being the primary ammonia source. Highest ammonia mixing ratios are found in the densely populated old city centre (Reche et al., 2015). Agriculture, waste management, and traffic are also all significant sources of low molecular weight alkylamines, such as DMA (Ábalos et al., 1999; Cadle and Mulawa, 1980; Hutchinson et al., 1982; Ge et al., 2011a), and are likely the source of amines found in this dataset. Activities such as composting and food industry are especially strong sources of trimethylamine (TMA) (Ge et al., 2011a). Although high emission fluxes of TMA are expected in this environment, they are not present in our spectra. The TMA ion has been reported previously with a similar ionisation setup to that utilised in this study (Kürten et al., 2016). On full-event days, the signal for C_2 and C_4 amines has a midday elevation concurrent with peaks to solar radiation (Figure S2), and can help explain the high formation rates we see in this dataset (see section 3.2). The relative strength of these signals are shown in Figure S3, with significantly higher signals attributed to ammonia compared to amines, despite a likely lower sensitivity (Simon et al., 2016).

HOM concentrations were greatly enhanced during full-event periods (factor of 1.5 higher compared to non-NPF mean), but lower during burst-event periods (factor of 1.2 lower compared to non-NPF mean), implying their necessity for growth. The sources and implications of these HOMs are discussed in section 3.3. Further, concentrations of iodine and DMS-derived acids such as iodic acid (HIO_3) and methanesulphonic acid (MSA) are low ($7.8 \cdot 10^5$ and $3.3 \cdot 10^5$ cm^{-3} respectively), indicating a small influence of oceanic emissions on particle nucleation/growth. Extended box plots as Figures 2 & 3 are presented in Figure S4, and HYSPLIT back trajectories per event in Figure S5.

3.2 Mechanisms of New Particle Formation

The correlation between $J_{1.9}$ and concentration of sulphuric acid is plotted in Figure 4. A close relationship between nucleation rates and sulphuric acid concentrations ($R^2 = 0.49$) are consistent with observations globally (Lee et al., 2019). This relationship is not dependent upon condensation sink. These NPF rates have no dependence on other ions as measured by CI-APi-ToF, including HIO_3, MSA, ammonia, amines or HOMs (R^2 for all <0.1). This is not to say that all of these molecules are not involved in the nucleation process, rather that elevations or reductions to their concentrations during nucleation periods do not have significant impact on nucleation rates. In the example of alkylamines, their gas phase concentration may decrease due to clustering with elevated sulphuric acid, as they cluster at around a 1:1 ratio at high amine mixing ratios (Kürten et al., 2014) (and therefore they will not be detectable as free amines). Further, if amines are present at a few pptv, their mixing ratios are significantly higher than our ambient measured sulphuric acid concentrations, and will be sufficient to accelerate nucleation rates (Almeida et al., 2013). Photochemical losses will also be greater during the periods of highest NPF rate (Ge et al., 2011b). The strength of the relationship between sulphuric acid and nucleation rate has been quantitatively reproduced in chamber studies involving the H_2SO_4-H_2O-DMA, and H_2SO_4-H_2O-BioOxOrg system, accurately reproducing tropospheric observations of nucleation rates (Almeida et al., 2013; Riccobono et al., 2014), although a later revision of the former shows nucleation rates at 278 K exceeding typical tropospheric observations in the presence of high mixing ratios of DMA (Kürten et al., 2018). A comparison between our data and results from the CLOUD chamber is presented in Figure 5; included are the H_2SO_4-H_2O, H_2SO_4-NH_3-H_2O (Kirkby et al., 2011), H_2SO_4-H_2O-DMA (Kürten et al., 2018) and H_2SO_4-BioOxOrg-H_2O systems (Riccobono et al., 2014) – BioOxOrg refers to the oxidation products of pinanediol ($C_{10}H_{18}O_2$) and $OH^{\cdot}$. Data from these chamber experiments is for 278 K and 38 - 39 % relative humidity. Nucleation rates measured in Barcelona ($J_{1.9}$ 178 ± 190 cm^{-3} s^{-1} at [H_2SO_4] $7.1\cdot10^6 \pm 2.7\cdot10^6$ cm^{-3}) are around an order of magnitude lower than that seen for the H_2SO_4-DMA-H_2SO_4 system , but exceed that of the H_2SO_4-BioOxOrg-H_2O system by ~1 order of magnitude, and that of the H_2SO_4-NH_3-H_2O and H_2SO_4-H_2O system multiple orders of magnitude. No dissimilarity is seen between the data points corresponding to full or burst type nucleation, indicating similar mechanisms of formation, despite lower HOM concentrations on burst-event days. Conversely, research in remote boreal environments show that the mechanism of nucleation can modulate dependent upon the H_2SO_4:HOM ratio (Yan et al., 2018). Model studies of sulphuric acid-amine nucleation show a decline in nucleation rate with temperature (Almeida et al., 2013; Olenius et al., 2017), as the evaporation rate of sulphuric acid-amine clusters will increase with temperature (Paasonen et al., 2012). Conversely, evaporation rates of such small clusters, and resultant nucleation rates tend to increase modestly with increases in relative humidity, most pronounced at lower amine concentrations (Almeida et al., 2013; Paasonen et al., 2012). Despite this, high nucleation rates at temperatures nearing 300 K have been reported previously (Kuang et al., 2008; Kürten et al., 2016), although these tend to show a temperature dependence (Yu et al., 2016). No higher-order sulphuric acid clusters, sulphuric acid-base clusters, nor sulphuric acid-HOM clusters were visible in the mass spectral data, likely due to these being below the limit of detection of the instrument (Jokinen et al., 2012), so cluster identity cannot be directly identified. Sulfuric acid trimer stabilisation is dependent upon base abundance (Ortega et al 2012), and conversely, sensitivity of nitrate CI-APi-ToF to sulfuric acid-base clusters is reduced due to the high base content of such clusters (Jen et al., 2016).

To further explore the relationship between sulphuric acid clusters and the rate of nucleation, the sulphuric acid dimer:monomer ratio is plotted in Figure 6. The sulphuric acid dimer:monomer ratio is elevated by the presence of gas-phase bases such as DMA, and this elevation is dependent upon both the abundances and proton affinities of such bases (Olenius et al., 2017). Upon charging, evaporation of water and bases from sulphuric acid clusters occurs, and thus these are detected as sulphuric acid dimer (Ortega et al., 2012, 2014). The binding energy of the bisulphate-H_2SO_4 ion is in excess of 40 kcal mol^{-1} (Curtius et al., 2001), and thus minimal declustering of the dimer is expected within the CI-APi-ToF instrument – however, declustering of higher order sulphuric acid clusters has been shown to be sensitive to voltage tune (Passanati et al., 2019), and this likely extends to the dimer also, and as such discrepancies between sets of results due to instrument setup cannot be ruled out. The ratio of sulphuric acid dimer:monomer is also highly sensitive to condensation sinks, with a difference in dimer concentration of approximately a factor of 4 expected at 10^7 cm^{-3} between 0.001 s^{-1} (a clean environment) and 0.03 s^{-1} (condensation sinks during these NPF events measured in this dataset) (Yao et al., 2018) and thus our low dimer:monomer ratio can, in part, be explained by elevated condensation sinks. The dashed line represents the ratio that would be seen due to ion induced clustering (IIC) in the nitrate chemical ionisation system for a 50 ms reaction time (Zhao et al., 2010). The sulphuric acid dimer:monomer ratio seen in the CLOUD H_2SO_4-DMA-H_2O system is plotted, alongside our own data from Barcelona. The ratio from our own data is seen to be much lower than that for the system purely involving DMA as a ternary stabilising species. Similarly, this ratio is lower than for reports of H_2SO_4-DMA-H_2O nucleation in Shanghai (Yao et al., 2018), but is markedly similar to reports in central rural Germany (Kürten et al., 2016). Similar to central Germany, this ratio increases at lower sulphuric acid concentrations to a ratio more similar to the H_2SO_4-DMA-H_2O system. A possible explanation for this is that at higher sulphuric acid concentrations, the concentrations of stronger stabilising bases are insufficient to stabilise all present sulphuric acid, with the higher end of the sulphuric acid concentrations seen in this data roughly equivalent to 1 pptv sulphuric acid (3×10^7

cm^{-3} = 1.2 pptv sulphuric acid). We also cannot account for clustering due to naturally charged sulphuric acid in the atmosphere, but ion concentrations in urban environments tend to be small due to efficient sink processes (Hirsikko et al., 2011). Particle formation plausibly operates by sulphuric acid-amine nucleation involving the measured C_2 and C_4 amines in our data, with nucleation rates hindered relative to those measured in the CLOUD experiments by elevated temperatures, and a decline to the sulphuric acid dimer:monomer ratio indicates that base concentrations may be limited. We cannot rule out an involvement of HOMs in particle formation processes, and, as no higher-order clusters were observed, we cannot establish sulphuric acid-amine nucleation with certainty.

3.3 HOMs and Growth

3.3.1 HOM composition and sources

Barcelona, as a densely populated urban agglomerate, is distinct from the remote conditions under which HOMs have primarily been studied (Bianchi et al., 2016, 2017; Schobesberger et al., 2013; Yan et al., 2016), and is characterised by elevated temperatures, insolation and NO_x mixing ratios, as well as a diverse host of potential precursor VOC. The first of these affects HOM yields significantly, as yields are highly dependent upon temperature (Quéléver et al., 2019; Stolzenburg et al., 2018). Lower temperatures result in slower H-abstractions, which will result in the likelihood of an $RO_2^{\cdot}$ to undergo a different reaction pathway, such as termination with $HO_2^{\cdot}$ to increase (Praske et al., 2018). This is particularly important in this study if there is a large energy barrier for the first or second H-abstraction taking place, as this will determine the number of hydrogen bond donating groups, and therefore whether the NO_3^- CI-APi-ToF is sensitive to a molecule or not. Elevated insolation will result in enhanced photochemistry, and thus more rapid $RO_2^{\cdot}$ formation rates, whereas elevated NO_x will produce more HOM with nitrate ester functionality (Garmash et al., 2019; Rissanen, 2018), which tend towards higher volatilities, and less efficient participation in particle formation (Ehn et al., 2014; Lehtipalo et al., 2018), and growth (Yao et al., 2020).

Oxygenated volatile organic compounds (OVOC) are defined as species visible in the nitrate CI-APi-ToF that do not classify as HOM. Here, the first of the three criteria provided by Bianchi et al. (2019), that HOM must be formed by peroxy radical autoxidation, cannot be applied to define HOM, as knowledge as to whether a molecule is a result of autoxidation requires sound knowledge of the structure of the precursors, oxidants and peroxy radical terminators present, however, the number of molecules observed with $nN = 2$ is around an order of magnitude lower than that for $nN = 1$, where the primary source of multiple nitrogen functionalities would be multiple peroxy radical termination reactions from NO_x, and therefore while multiple generations of oxidation have been shown to occur in aromatics (Garmash et al., 2020), it is a small contributor to the concentration of what is classed as HOM here. The second criterion to define HOM are that they must be formed in the gas phase under atmospherically relevant conditions, which we deem appropriately fulfilled as all CI-APi-ToF measurements are of gas phase compounds, and the final criterion is that HOM must contain more than 6 oxygen atoms. To attempt to satisfy these criteria as best possible, the criteria of both containing 6 oxygen atoms and 5 carbon atoms or greater and having an O:C ratio >0.6 is applied.

The diversified range of HOM precursors in Barcelona will be primarily anthropogenic in origin. Averaged PTR-MS mixing ratios of different VOCs are presented in Figure S6. Figure 7(a) shows HOM concentration plotted against temperature, showing a dependence of HOM concentrations on temperature, with a lesser dependence on global radiation. The precursors for these HOMs are presumed to be largely isoprene, alkylbenzenes, monoterpenes, and PAHs. The mean peak intensities assigned to alkylbenzene derived HOMs are approximately a factor of two higher than those assigned to isoprene and monoterpene oxidation across this entire campaign. In this data these VOC mixing ratios are, with the exception of isoprene, not largely temperature dependent, with many of these HOMs forming under negligible or zero insolation, and therefore very low $OH^{\cdot}$ concentrations. These nighttime HOMs will not be derived from the oxidation of aromatics, however, as rates of oxidation of alkylbenzenes by O_3 and $NO_3^·$ are negligible (Molteni et al, 2018). These nighttime HOMs will therefore mostly be derived from biogenic emissions which undergo more rapid nocturnal oxidation, and are likely transported from inland by the land breeze during night (Millán, 2014; Querol et al., 2017).

Operating under the assumption that C_5, C_6, C_7, C_8, and C_9 HOMs primarily arise from isoprene, benzene toluene, C_2-alkylbenzene C_3-alkylbenzene oxidation respectively (Massoli et al., 2018; Molteni et al., 2018; Wang et al., 2017), HOM signals plotted against parent VOC concentration indicate their dependence upon that VOC. Here, a C_7 HOM is thought to follow the formula $C_7H_{8-12}O_{5-10}N_{0-2}$. We have plotted HOM concentrations against VOC concentrations in Figure 7(b). C_{10} HOMs are not included in these analyses as these may primarily arise from $C_{10}H_{12-14}$ alkylbenzene, or monoterpene oxidation. HOM concentration appears mostly independent of VOC concentration, with the exception of isoprene, for which emissions are highly temperature dependent, and thus this is likely a function of the effect of temperature on HOM formation (Figure 7(a)). A lack of correlation between other VOCs and their HOMs confirms that this relationship between HOMs and temperature is not a function of enhanced VOC emission fluxes from, for example, evaporation, except in the instance of isoprene. Fragmented monoterpene oxidation products will also contribute to the total number of C_9 HOMs, and similarly, other VOCs can fragment upon oxidation. However, these results indicate that HOM concentrations are elevated by temperature, and operate quite independent of precursor VOC concentration.

DBE as calculated by equation 3 is equal to the number of pi bonds and rings within a molecule. Benzene, toluene, and similar aromatics have DBE = 4, naphthalene = 7 and monoterpenes = 3. DBE can be used as an indicator of sources when considering HOM in bulk. Saturation mass concentration as calculated by equation 4 can help describe capacity of a molecule to both condense onto newly formed particles and participate in nucleation. Figure 8 shows concentrations of HOMs and other oxygenated organic molecules binned to the nearest integer $\mathrm{Log}_{10}(C^*)(300\ \mathrm{K})$, coloured by DBE. Mean ion signals per carbon number are shown in Figure S7. Most measured molecules fall into the SVOC class ($0.3 < C^*(300\ \mathrm{K}) < 300\ \mu\mathrm{g\ m}^{-3}$) which will mostly exist in equilibrium between gas and particle phase. Highest SVOC concentrations arise from fingerprint molecules for isoprene oxidation under high NO_x ($C_5H_{10}N_2O_8$) (Brean et al., 2019), and oxidation of small alkylbenzenes ($C_7H_8O_5$, $C_8H_{10}O_5$). LVOC and ELVOC ($3\cdot10^{-5} < C^* < 0.3\ \mu\mathrm{g\ m}^{-3}$ and $3\cdot10^{-9} < C^*(300\ \mathrm{K}) < 3\cdot10^{-5}\ \mu\mathrm{g\ m}^{-3}$ respectively) have a greater contribution from molecules with higher DBE, i.e., $C_{10}H_{10}O_8$ arising most likely from PAH oxidation (Molteni et al., 2018), and $C_{10}H_{15}O_7N$, a common molecule arising from monoterpene oxidation in the presence of NO_x. The contribution of molecules with carbon number ≤ 9 to these LVOC is modest, and ELVOCs are entirely comprised of molecules with carbon numbers ≥ 10, and is dominated by DBEs of 8 and 4, attributable to PAH and monoterpene oxidation respectively. No molecules classed as ultra-low volatility organic compounds (ULVOC, $C^*(300\ \mathrm{K}) < 3\cdot10^{-9}\ \mu\mathrm{g\ m}^{-3}$) were observed in our data, and thus any pure HOM nucleation is unlikely.

3.3.2 HOMs and NPF

As shown in Figure 3, an elevated HOM concentration appears to be a necessary condition for particle growth past 10 nm during NPF events. These days are associated with elevated temperatures, solar radiation, higher ozone, and lower $NO:NO_2$ ratio. HIO_3 is also significantly higher on burst-event days. A recent study in a remote environment reports growth rates matching condensation rates without accounting for aqueous phase chemistry (Mohr et al., 2019). From 2D-VBS volatility calculations discussed in the previous section, is it shown that LVOC and ELVOC measured in Barcelona plausibly arise from the oxidation of aromatics (particularly PAHs in the case of ELVOC) and monoterpenes. Calculated growth rates according to the method of Nieminen et al. (2010) are presented in Figure S8 for both $GR_{1.9-5}$ and GR_{5-20}. Best agreement for GR_{5-20} is when condensation of SVOC, LVOC, ELVOC, MSA, HIO_3 and H_2SO_4 is considered, and best agreement for $GR_{1.9-5}$ is seen for condensation of all these except SVOC. The uncertainties in this method are large, and assumptions of irreversible condensation of SVOC onto particles of 5 nm likely lead to overestimations; however, these results indicate an essential role of the condensation of organic compounds to produce high growth rates observed in urban environments.

Figure 9 shows three mass-defect plots for a non-event period, full-event period, and burst-event period. The non-event day included in Figure 8 was characterised by lower solar radiation and temperatures than average, so lower signals for oxygenated species are seen due to weaker photochemistry (i.e., $OH^{\cdot}$ concentration), and slower autoxidation due to slower H-shift reactions (Frege et al., 2018; Quéléver et al., 2019; Stolzenburg et al., 2018). The full-event day sees enhancements to smaller OVOCs and HOMs compared to the non-event day, especially around 150-200 m/Q, which contains peaks corresponding to dicarboxylic acids and isoprene oxidation products. Some of the largest peaks in the mass spectra correspond to formulae seen arising from the enhanced $OH^{\cdot}$ oxidation of alkylbenzenes (such as $C_7H_7NO_6$) (Molteni et al., 2018; Wang et al., 2017). Larger HOMs see a less significant enhancement to smaller alkylbenzene derived HOMs. The presence of larger, unidentified HOMs >400 m/Q is enhanced during full-events, these peaks will comprise the largest compounds, most likely of class ELVOC, arising from the oxidation of large VOCs, or $RO_2^{\cdot}$-$RO_2^{\cdot}$ accretion reactions, and thus, we likely underpredict ELVOC concentrations and resultant impacts on particle growth in Figure S8. These unidentified peaks >400 m/Q are both more numerous and larger during full-event periods, with a factor of two difference in total peak area. The burst-event day has significantly lower concentrations of OVOCs and HOMs, and to a lesser degree, their nitrogen containing counterparts (N-OVOCs and N-HOMs), with significantly fewer compounds >400 m/Q. The most significant difference between full and burst-event days is in the SVOCs, accounting for a factor of two difference in concentration. The sulphur containing acids all have similar peak areas to the full-event day. These elevations to condensable OVOCs and HOMs on particle formation days with growth are consistent with particle composition data as measured by ACSM (Figure S9). Particle composition on full-event days shows an elevation to organic mass concentration in the late evening and night around when new particles from NPF will reach sizes detectable by the ACSM (~75 nm, Ng et al., 2011). Organic mass between 16:00 – 23:00 is 3.5 µg m^{-3} on burst-event days, versus 7.8 µg m^{-3} on full-event days.

4. CONCLUSIONS

We show new particle formation rates in Barcelona are linearly dependent upon the sulphuric acid concentrations, and while formation rates far exceed that of H_2SO_4-BioOxOrg-H_2O nucleation, they fall short of those of H_2SO_4-DMA-H_2O nucleation at 278 K, as does the sulphuric acid dimer:monomer ratio, possibly explained by cluster evaporation due to high temperatures in summertime Barcelona (303 K during events), and limited pools of gas-phase amines. These results are similar to reports of nucleation rates in rural Germany (Kürten et al., 2016). As no higher-order clusters were directly measured, we cannot determine nucleation mechanisms with certainty, and an involvement of HOMs in nucleation is plausible.

High concentrations of OVOCs and HOMs were measured by CI-APi-ToF. Of these, the SVOC arose from mostly isoprene and alkylbenzene oxidation, whereas LVOC and ELVOC arose from alkylbenzene, monoterpene and PAH oxidation together, with a dependence of their concentration on temperature. Concentrations of species associated with coastal and oceanic sources such as MSA and HIO_3 were low. High HOM signals are seen to be a necessary condition for new particle growth past 10 nm, with the most significant difference between days with and without particle growth being SVOC concentrations (factor of 2 difference), while modelled growth rates from condensation of these organic compounds, alongside H_2SO_4, MSA and HIO_3 were shown to match growth rates within measurement error. Thus, oxidation of traffic derived alkylbenzenes and PAHs, and to a lesser degree, isoprene and monoterpene emissions is a significant determinant of new particle growth in this environment.

These results are consistent with extensive chamber and flow tube studies on particle formation from sulphuric acid, amines and HOMs, and further, nucleation rates relative to sulphuric acid are similar to many tropospheric observations. Barcelona is representative of many Mediterranean urban environments, with moderate pollution, influence of shipping emissions, and high insolation, and the present study reveals the complexity of NPF mechanisms in these environments.

DATA AVAILABILITY

Data supporting this publication are openly available from the UBIRA eData repository at https://doi.org/10.25500/edata.bham.00000434

AUTHOR CONTRIBUTIONS

RMH and XQ conceived the study, JB and DCSB carried out the CI-APi-TOF and related measurements with assistance from AA and MCM. The VOC measurements were proposed by NM and collected by BT-R. JB wrote the first draft of the manuscript which was enhanced by contributions from the co-authors.

COMPETING INTERESTS

The authors have no conflict of interests.

ACKNOWLEDGEMENTS

Financial assistance from the Spanish Ministry of Science, Innovation and Universities and Competitiveness and FEDER funds under the project HOUSE (CGL2016-78594-R), and by the Generalitat de Catalunya (AGAUR 2017 SGR41) is gratefully acknowledged. MCM acknowledges the Ramón y Cajal Fellowship awarded by the Spanish Ministry. Financial support of the UK scientists by the Natural Environment Research Council through the National Centre for Atmospheric Science is also acknowledged (R8/H12/83/011).

FIGURE LEGENDS:

Figure 1: Average SMPS contour plots for (a) non-event days, (b) full-event days and (c) burst-event days.

Figure 2: Box plots for days of non-event, full-event and burst-event, showing (a) condensation sink, (b) temperature, and (c) global radiation from hourly data. “Full-event” and “burst-event” include data across the entire day.

Figure 3: Box plots for days of non-event, full-event and burst-event, showing (a) sulphuric acid, (b) C_2 and C_4 amines, as clustered with the nitrate dimer and trimer, and (c) summed HOM concentration from C_5+ from hourly data. Units for ammonia + amines are normalised counts, as no calibration was performed. Event days include data across the full event day.

Figure 4: Formation rate ($J_{1.9}$) plotted against sulphuric acid monomer concentration, coloured by condensation sink. Circles represent burst-events, squares represent full events. Data is for hourly averages across NPF periods, typically within the hours 08:00 – 16:00. Slope of the line = $4.9 \cdot 10^{-5}$ s^{-1}. Error bars represent systematic uncertainties on [H_2SO4] and $J_{1.9}$

Figure 5: Formation rate plotted against sulphuric acid monomer concentration for data collected from Barcelona. Tan circles represent burst-events, purple squares represent full events. as well as that for the H_2SO_4-H_2O (blue inverted triangles), H_2SO_4-NH_3-H_2O (yellow inverted triangles), H_2SO_4-DMA-H_2O (pink triangles), and H_2SO_4-BioOxOrg-H_2O (brown diamonds) systems from the CLOUD chamber (Kürten et al., 2018 Kirkby et al., 2011; Riccobono et al., 2014). CLOUD chamber experiments were performed at 278 K and 38 – 39 % RH. Data is for hourly averages across NPF periods, typically within the hours 08:00 – 16:00. Error bars represent systematic uncertainties on [H_2SO_4] and $J_{1.9}$.

Figure 6: Sulphuric acid dimer concentration plotted against monomer concentration, showing burst-event periods (tan circles), full event periods (purple squares), non-event periods (green inverted triangles), and the ratio of sulphuric acid dimer:monomer in the CLOUD chamber for the H_2SO_4-H_2O-DMA system (pink triangles) (Almeida et al., 2013). Dashed line represents the dimer concentration produced by ion induced clustering in the chemical ionization unit (Zhao et al., 2010). CLOUD chamber experiments were performed at 278 K and 38 – 39 % RH. Data is for hourly averages across NPF periods, typically within the hours 08:00 – 16:00. Error bars represent systematic uncertainties on [H_2SO_4] and [$(H_2SO_4)_2$].

Figure 7: Influencing factors on HOM concentration, showing (a) $C_{5\text{-}10}$ HOM concentration plotted against temperature, coloured by global radiation. Ellipsis shows 95% confidence on a multivariate t-distribution. (b) HOM concentration by carbon number potted against parent VOC mixing ratio. These are segregated by carbon number/VOC, i.e, C_7 HOMs plotted against toluene, under the assumption that toluene oxidation is the main producer of C_7 HOMs. Time for both plots is of hourly time resolution.

Figure 8: Concentrations of all oxygenated organic molecules and HOMs binned to integer $\mathrm{Log}_{10}(C^*)$ values, coloured by DBE.

Figure 9: Mass defect plots for (a) non-event, (b) full-event, and (c) burst-event periods, data taken from 10:00 – 15:00 on the days 11/07/2018, 16/07/2018 and 15/07/2018 respectively. Size corresponds to mass spectral peak area. Ions are coloured according to identified chemical composition. *Blue* points correspond to HOMs containing all organic species with ≥5 carbon atoms and ≥6 oxygen atoms, and an O:C ratio of >0.6. *Purple* points correspond to the same but for species containing 1-2 nitrogen atoms. Species not meeting this HOM criterea were classed generally as OVOCs which are coloured *brown*, with the nitrogen containing OVOCs coloured *orange*. Sulphur acids (*red*) include ions HSO_4^-, $CH_3SO_3^-$ and SO_5^-, as well as the sulphuric acid dimer. Iodine acids (*green*) contains both IO_3^- and I^- (the latter presumably deprotonated hydrogen iodide). Unidentified points are left uncoloured.

REFERENCES

Ábalos, M., Bayona, J. M. and Ventura, F.: Development of a solid-phase microextraction GC-NPD procedure for the determination of free volatile amines in wastewater and sewage-polluted waters, Anal. Chem., 71(16), 3531–3537, doi:10.1021/ac990197h, 1999.

Almeida, J., Schobesberger, S., Kürten, A., Ortega, I. K., Kupiainen-Määttä, O., Praplan, A. P., Adamov, A., Amorim, A., Bianchi, F., Breitenlechner, M., David, A., Dommen, J., Donahue, N. M., Downard, A., Dunne, E., Duplissy, J., Ehrhart, S., Flagan, R. C., Franchin, A., Guida, R., Hakala, J., Hansel, A., Heinritzi, M., Henschel, H., Jokinen, T., Junninen, H., Kajos, M., Kangasluoma, J., Keskinen, H., Kupc, A., Kurtén, T., Kvashin, A. N., Laaksonen, A., Lehtipalo, K., Leiminger, M., Leppä, J., Loukonen, V., Makhmutov, V., Mathot, S., McGrath, M. J., Nieminen, T., Olenius, T., Onnela, A., Petäjä, T., Riccobono, F., Riipinen, I., Rissanen, M., Rondo, L., Ruuskanen, T., Santos, F. D., Sarnela, N., Schallhart, S., Schnitzhofer, R., Seinfeld, J. H., Simon, M., Sipilä, M., Stozhkov, Y., Stratmann, F., Tomé, A., Tröstl, J., Tsagkogeorgas, G., Vaattovaara, P., Viisanen, Y., Virtanen, A., Vrtala, A., Wagner, P. E., Weingartner, E., Wex, H., Williamson, C., Wimmer, D., Ye, P., Yli-Juuti, T., Carslaw, K. S., Kulmala, M., Curtius, J., Baltensperger, U., Worsnop, D. R., Vehkamäki, H. and Kirkby, J.: Molecular understanding of sulphuric acid-amine particle nucleation in the atmosphere, Nature, 502(7471), 359–363, doi:10.1038/nature12663, 2013.

Bianchi, F., Tröstl, J., Junninen, H., Frege, C., Henne, S., Hoyle, C. R., Molteni, U., Herrmann, E., Bukowiecki, N., Chen, X., Duplissy, J., Gysel, M., Hutterli, M., Kangasluoma, J., Kontkanen, J., Manninen, H. E., Münch, S., Peräkylä, O., Petäjä, T., Rondo, L., Williamson, C., Weingartner, E., Worsnop, D. R., Kulmala, M., Dommen, J. and Baltensperger, U.: New particle formation in the free troposphere : A question of chemistry and timing, Science (80-.)., 5456(May), 1–11, 2016.

Bianchi, F., Garmash, O., He, X., Yan, C., Iyer, S., Rosendahl, I., Xu, Z., Rissanen, M. P., Riva, M., Taipale, R., Sarnela, N., Petäjä, T., Worsnop, D. R., Kulmala, M., Ehn, M. and Junninen, H.: The role of highly oxygenated molecules (HOMs) in determining the composition of ambient ions in the boreal forest, Atmos. Chem. Phys., 17(22), 13819–13831, doi:10.5194/acp-17-13819-2017, 2017.

Bianchi, F., Kurtén, T., Riva, M., Mohr, C., Rissanen, M. P., Roldin, P., Berndt, T., Crounse, J. D., Wennberg, P. O., Mentel, T. F., Wildt, J., Junninen, H., Jokinen, T., Kulmala, M., Worsnop, D. R., Thornton, J. A., Donahue, N., Kjaergaard, H. G. and Ehn, M.: Highly Oxygenated Organic Molecules (HOM) from Gas-Phase Autoxidation Involving Peroxy Radicals: A Key Contributor to Atmospheric Aerosol, Chem. Rev., 2019.

Bousiotis, D., Dall'osto, M., Beddows, D. C. S., Pope, F. D. and Harrison, R. M.: Analysis of new particle formation (NPF) events at nearby rural, urban background and urban roadside sites, Atmos. Chem. Phys, 19, 5679–5694, doi:10.5194/acp-19-5679-2019, 2019.

Brean, J., Harrison, R. M., Shi, Z., Beddows, D. C. S., W Joe, A. F. and Nicholas Hewitt, C.: Observations of highly oxidised molecules and particle nucleation in the atmosphere of Beijing, Atmos. Chem. Phys. Discuss., (March), 1–35, doi:10.5194/acp-2019-156, 2019.

Brines, M., Dall'Osto, M., Beddows, D. C. S., Harrison, R. M., and Querol, X.: Simplifying aerosol size distributions modes simultaneously detected at four monitoring sites during SAPUSS, Atmos. Chem. Phys., 14, 2973–2986, https://doi.org/10.5194/acp-14-2973-2014, 2014.

Brines, M., Dall'Osto, M., Beddows, D. C. S., Harrison, R. M., Gómez-Moreno, F., Núñez, L., Artíñano, B., Costabile, F., Gobbi, G. P., Salimi, F., Morawska, L., Sioutas, C., and Querol, X.:

Traffic and nucleation events as main sources of ultrafine particles in high-insolation developed world cities, Atmos. Chem. Phys., 15, 5929–5945, https://doi.org/10.5194/acp-15-5929-2015, 2015.

Cadle, S. H. and Mulawa, P. A.: Low-molecular-weight aliphatic amines in exhaust from catalyst-equipped cars, Environ. Sci. Technol., 14(6), 718–723, doi:10.1021/es60166a011, 1980.

Carnerero, C., Pérez, N., Petäjä, T., Laurila, T. M., Ahonen, L. R., Kontkanen, J., Ahn, K. H., Alastuey, A. and Querol, X.: Relating high ozone, ultrafine particles, and new particle formation episodes using cluster analysis, Atmos. Environ. X, 4(May), 1–20, doi:10.1016/j.aeaoa.2019.100051, 2019.

Cohen, A. J., Brauer, M., Burnett, R., Anderson, H. R., Frostad, J., Estep, K., Balakrishnan, K., Brunekreef, B., Dandona, L., Dandona, R., Feigin, V., Freedman, G., Hubbell, B., Jobling, A., Kan, H., Knibbs, L., Liu, Y., Martin, R., Morawska, L., Pope, C. A., Shin, H., Straif, K., Shaddick, G., Thomas, M., van Dingenen, R., van Donkelaar, A., Vos, T., Murray, C. J. L. and Forouzanfar, M. H.: Estimates and 25-year trends of the global burden of disease attributable to ambient air pollution: an analysis of data from the Global Burden of Diseases Study 2015, Lancet, 389(10082), 1907–1918, doi:10.1016/S0140-6736(17)30505-6, 2017.

Cubison, M. J. and Jimenez, J. L.: Statistical precision of the intensities retrieved from constrained fitting of overlapping peaks in high-resolution mass spectra, Atmos. Meas. Tech., 8(6), 2333–2345, doi:10.5194/amt-8-2333-2015, 2015.

Curtius, J., Froyd, K. D. and Lovejoy, E. R.: Cluster ion thermal decomposition (I): Experimental kinetics study and ab initio calculations for $HSO_4^-(H_2SO_4)_x(HNO_3)_y$, J. Phys. Chem. A, 105(48), 10867–10873, doi:10.1021/jp0124950, 2001.

Dal Maso, M., Kulmala, M., Riipinen, I., Wagner, R., Hussein, T., Aalto, P. P. and Lehtinen, K. E. J.: Formation and growth of fresh atmospheric aerosols: Eight years of aerosol size distribution data from SMEAR II, Hyytiälä, Finland, Boreal Environ. Res., 10(5), 323–336, 2005.

Dall'Osto, M., Querol, X., Alastuey, A., O'Dowd, C., Harrison, R. M., Wenger, J. and Gómez-Moreno, F. J.: On the spatial distribution and evolution of ultrafine particles in Barcelona, Atmos. Chem. Phys., 13(2), 741–759, doi:10.5194/acp-13-741-2013, 2013.

Donahue, N. M., Epstein, S. A., Pandis, S. N. and Robinson, A. L.: Atmospheric Chemistry and Physics A two-dimensional volatility basis set: 1. organic-aerosol mixing thermodynamics, Atmos. Chem. Phys, 11, 3303–3318, doi:10.5194/acp-11-3303-2011, 2011.

Ehn, M., Thornton, J. A., Kleist, E., Sipilä, M., Junninen, H., Pullinen, I., Springer, M., Rubach, F., Tillmann, R., Lee, B., Lopez-Hilfiker, F., Andres, S., Acir, I.-H., Rissanen, M., Jokinen, T., Schobesberger, S., Kangasluoma, J., Kontkanen, J., Nieminen, T., Kurtén, T., Nielsen, L. B., Jørgensen, S., Kjaergaard, H. G., Canagaratna, M., Maso, M. D., Berndt, T., Petäjä, T., Wahner, A., Kerminen, V.-M., Kulmala, M., Worsnop, D. R., Wildt, J. and Mentel, T. F.: A large source of low-volatility secondary organic aerosol, Nature, 506(7489), 476–479, doi:10.1038/nature13032, 2014.

Elm, J., Myllys, N. and Kurtén, T.: What is Required for Highly Oxidized Molecules to Form Clusters with Sulphuric Acid?, J. Phys. Chem. A, 121(23), 4578–4587, doi:10.1021/acs.jpca.7b03759, 2017.

Frege, C., Ortega, I. K., Rissanen, M. P., Praplan, A. P., Steiner, G., Heinritzi, M., Ahonen, L., Amorim, A., Bernhammer, A. K., Bianchi, F., Brilke, S., Breitenlechner, M., Dada, L., Dias, A., Duplissy, J., Ehrhart, S., El-Haddad, I., Fischer, L., Fuchs, C., Garmash, O., Gonin, M., Hansel, A., Hoyle, C. R., Jokinen, T., Junninen, H., Kirkby, J., Kürten, A., Lehtipalo, K., Leiminger, M., Lee

Mauldin, R., Molteni, U., Nichman, L., Petäjä, T., Sarnela, N., Schobesberger, S., Simon, M., Sipilä, M., Stolzenburg, D., Tomé, A., Vogel, A. L., Wagner, A. C., Wagner, R., Xiao, M., Yan, C., Ye, P., Curtius, J., Donahue, N. M., Flagan, R. C., Kulmala, M., Worsnop, D. R., Winkler, P., Dommen, J. and Baltensperger, U.: Influence of temperature on the molecular composition of ions and charged clusters during pure biogenic nucleation, Atmos. Chem. Phys., 18(1), 65–79, doi:10.5194/acp-18-65-2018, 2018.

Garmash, O., Rissanen, M. P., Pullinen, I., Schmitt, S., Kausiala, O., Tillmann, R., Zhao, D., Percival, C., Bannan, T. J., Priestley, M., Hallquist, Å. M., Kleist, E., Kiendler-Scharr, A., Hallquist, M., Berndt, T., McFiggans, G., Wildt, J., Mentel, T. F., and Ehn, M.: Multi-generation OH oxidation as a source for highly oxygenated organic molecules from aromatics, Atmos. Chem. Phys., 20, 515–537, https://doi.org/10.5194/acp-20-515-2020, 2020.

Ge, X., Wexler, A. S. and Clegg, S. L.: Atmospheric amines - Part I. A review, Atmos. Environ., 45(3), 524–546, doi:10.1016/j.atmosenv.2010.10.012, 2011a.

Ge, X., Wexler, A. S. and Clegg, S. L.: Atmospheric amines - Part II. Thermodynamic properties and gas/particle partitioning, Atmos. Environ., 45(3), 561–577, doi:10.1016/j.atmosenv.2010.10.013, 2011b.

Glasoe, W. A., Volz, K., Panta, B., Freshour, N., Bachman, R., Hanson, D. R., Mcmurry, P. H. and Jen, C.: Sulphuric acid nucleation: An experimental study of the effect of seven bases, J. Geophys. Res. Atmos., 175(120), 1933–1950, doi:10.1038/175238c0, 2015.

Graus, M., Müller, M. and Hansel, A.: High resolution PTR-TOF: Quantification and Formula Confirmation of VOC in Real Time, J. Am. Soc. Mass Spectrom., 21(6), 1037–1044, doi:10.1016/j.jasms.2010.02.006, 2010.

Guo, S., Hu, M., Zamora, M. L., Peng, J., Shang, D., Zheng, J., Du, Z., Wu, Z., Shao, M., Zeng, L., Molina, M. J. and Zhang, R.: Elucidating severe urban haze formation in China., Proc. Natl. Acad. Sci. U. S. A., 111(49), 17373–8, doi:10.1073/pnas.1419604111, 2014.

Harrison, R. M., Rob Mackenzie, A., Xu, H., Alam, M. S., Nikolova, I., Zhong, J., Singh, A., Zeraati-Rezaei, S., Stark, C., Beddows, D. C. S., Liang, Z., Xu, R. and Cai, X.: Diesel exhaust nanoparticles and their behaviour in the atmosphere, Proc. R. Soc. A Math. Phys. Eng. Sci., 474(2220), doi:10.1098/rspa.2018.0492, 2018.

Henschel, S., Querol, X., Atkinson, R., Pandolfi, M., Zeka, A., Tertre, A. L., Analistis, A., Katsouyanni, K., Chanel, O., Pascal, M., Bouland, C., Haluza, D., Medina, S., and Goodman, P. G.: Ambient air SO2 patterns in 6 European cities, Atmos. Environ., 79, 236–247, https://doi.org/10.1016/j.atmosenv.2013.06.008, 2013.

Hirsikko, A., Nieminen, T., Gagné, S., Lehtipalo, K., Manninen, H. E., Ehn, M., Hõrrak, U., Kerminen, V.-M., Laakso, L., Mcmurry, P. H., Mirme, A., Mirme, S., Petäjä, T., Tammet, H., Vakkari, V., Vana, M. and Kulmala, M.: Atmospheric ions and nucleation: a review of observations, Atmos. Chem. Phys, 11, 767–798, doi:10.5194/acp-11-767-2011, 2011.

Hutchinson, G. L., Mosier, A. R. and Andre, C. E.: Ammonia and Amine Emissions from a Large Cattle Feedlot, J. Environ. Qual., 11(2), 288–293, 1982.

Hyttinen, N., Kupiainen-Määtta, O., Rissanen, M. P., Muuronen, M., Ehn, M. and Kurtén, T.: Modeling the Charging of Highly Oxidized Cyclohexene Ozonolysis Products Using Nitrate-Based

Chemical Ionization, J. Phys. Chem. A, 119(24), 6339–6345, doi:10.1021/acs.jpca.5b01818, 2015.

IPCC, 2013: Climate Change 2013: The Physical Science Basis. Contribution of Working Group I to the Fifth Assessment Report of the Intergovernmental Panel on Climate Change, edited by V. B. and P. M. M. Stocker, T.F., D. Qin, G.-K. Plattner, M. Tignor, S.K. Allen, J. Boschung, A. Nauels, Y. Xia, Cambridge University Press, Cambridge., 2014.

Jen, C. N., Zhao, J., McMurry, P. H., and Hanson, D. R.: Chemical ionization of clusters formed from sulfuric acid and dimethylamine or diamines, Atmos. Chem. Phys., 16, 12513–12529, https://doi.org/10.5194/acp-16-12513-2016, 2016.

Jokinen, T., Sipilä, M., Junninen, H., Ehn, M., Lönn, G., Hakala, J., Petäjä, T., Mauldin, R. L., Kulmala, M. and Worsnop, D. R.: Atmospheric sulphuric acid and neutral cluster measurements using CI-APi-TOF, Atmos. Chem. Phys., 12(9), 4117–4125, doi:10.5194/acp-12-4117-2012, 2012.

Jokinen, T., Sipilä, M., Kontkanen, J., Vakkari, V., Tisler, P., Duplissy, E.-M., Junninen, H., Kangasluoma, J., Manninen, H. E., Petäjä, T., Kulmala, M., Worsnop, D. R., Kirkby, J., Virkkula, A. and Kerminen, V.-M.: Ion-induced sulphuric acid–ammonia nucleation drives particle formation in coastal Antarctica, Sci. Adv., 4(11), eaat9744, doi:10.1126/sciadv.aat9744, 2018.

Junninen, H., Ehn, M., Petäjä, Luosujärvi, L., Kotiaho, T., Kostiainen, R., Rohner, U., Gonin, M., Fuhrer, K., Kulmala, M. and Worsnop, D. R.: A high-resolution mass spectrometer to measure atmospheric ion composition, Atmos. Meas. Tech., 3(4), 1039–1053, doi:10.5194/amt-3-1039-2010, 2010.

Kerminen, V. M., Chen, X., Vakkari, V., Petäjä, T., Kulmala, M. and Bianchi, F.: Atmospheric new particle formation and growth: Review of field observations, Environ. Res. Lett., 13(10), doi:10.1088/1748-9326/aadf3c, 2018.

Kirkby, J., Curtius, J., Almeida, J., Dunne, E., Duplissy, J., Ehrhart, S., Franchin, A., Gagné, S., Ickes, L., Kürten, A., Kupc, A., Metzger, A., Riccobono, F., Rondo, L., Schobesberger, S., Tsagkogeorgas, G., Wimmer, D., Amorim, A., Bianchi, F., Breitenlechner, M., David, A., Dommen, J., Downard, A., Ehn, M., Flagan, R. C., Haider, S., Hansel, A., Hauser, D., Jud, W., Junninen, H., Kreissl, F., Kvashin, A., Laaksonen, A., Lehtipalo, K., Lima, J., Lovejoy, E. R., Makhmutov, V., Mathot, S., Mikkilä, J., Minginette, P., Mogo, S., Nieminen, T., Onnela, A., Pereira, P., Petäjä, T., Schnitzhofer, R., Seinfeld, J. H., Sipilä, M., Stozhkov, Y., Stratmann, F., Tomé, A., Vanhanen, J., Viisanen, Y., Vrtala, A., Wagner, P. E., Walther, H., Weingartner, E., Wex, H., Winkler, P. M., Carslaw, K. S., Worsnop, D. R., Baltensperger, U. and Kulmala, M.: Role of sulphuric acid, ammonia and galactic cosmic rays in atmospheric aerosol nucleation, Nature, 476(7361), 429–435, doi:10.1038/nature10343, 2011.

Kirkby, J., Duplissy, J., Sengupta, K., Frege, C., Gordon, H., Williamson, C., Heinritzi, M., Simon, M., Yan, C., Almeida, J., Trostl, J., Nieminen, T., Ortega, I. K., Wagner, R., Adamov, A., Amorim, A., Bernhammer, A. K., Bianchi, F., Breitenlechner, M., Brilke, S., Chen, X., Craven, J., Dias, A., Ehrhart, S., Flagan, R. C., Franchin, A., Fuchs, C., Guida, R., Hakala, J., Hoyle, C. R., Jokinen, T., Junninen, H., Kangasluoma, J., Kim, J., Krapf, M., Kurten, A., Laaksonen, A., Lehtipalo, K., Makhmutov, V., Mathot, S., Molteni, U., Onnela, A., Perakyla, O., Piel, F., Petaja, T., Praplan, A. P., Pringle, K., Rap, A., Richards, N. A. D., Riipinen, I., Rissanen, M. P., Rondo, L., Sarnela, N., Schobesberger, S., Scott, C. E., Seinfeld, J. H., Sipila, M., Steiner, G., Stozhkov, Y., Stratmann, F., Tomé, A., Virtanen, A., Vogel, A. L., Wagner, A. C., Wagner, P. E., Weingartner, E., Wimmer, D., Winkler, P. M., Ye, P., Zhang, X., Hansel, A., Dommen, J., Donahue, N. M., Worsnop, D. R., Baltensperger, U., Kulmala, M., Carslaw, K. S. and Curtius, J.: Ion-induced nucleation of pure biogenic particles, Nature, 533(7604), 521–526, doi:10.1038/nature17953, 2016.

Kuang, C., McMurry, P. H., McCormick, A. V. and Eisele, F. L.: Dependence of nucleation rates on sulfuric acid vapor concentration in diverse atmospheric locations, J. Geophys. Res. Atmos., 113(10), 1–9, doi:10.1029/2007JD009253, 2008.

Kulmala, M., Dal Maso, M., Mäkelä, J. M., Pirjola, L., Väkevä, M., Aalto, P., Miikkulainen, P., Hämeri, K. and O'Dowd, C. D.: On the formation, growth and composition of nucleation mode particles, Tellus, Ser. B Chem. Phys. Meteorol., 53(4), 479–490, doi:10.1034/j.1600-0889.2001.d01-33.x, 2001.

Kulmala, M., Petäjä, T., Nieminen, T., Sipilä, M., Manninen, H. E., Lehtipalo, K., Dal Maso, M., Aalto, P. P., Junninen, H., Paasonen, P., Riipinen, I., Lehtinen, K. E. J., Laaksonen, A. and Kerminen, V.-M.: Measurement of the nucleation of atmospheric aerosol particles, Nat. Protoc., 7(9), 1651–1667, doi:10.1038/nprot.2012.091, 2012.

Kulmala, M., Kerminen, V. M., Petäjä, T., Ding, A. J. and Wang, L.: Atmospheric gas-to-particle conversion: Why NPF events are observed in megacities?, Faraday Discuss., 200, 271–288, doi:10.1039/c6fd00257a, 2017.

Kürten, A., Jokinen, T., Simon, M., Sipilä, M., Sarnela, N., Junninen, H., Adamov, A., Almeida, J., Amorim, A., Bianchi, F., Breitenlechner, M., Dommen, J., Donahue, N. M., Duplissy, J., Ehrhart, S., Flagan, R. C., Franchin, A., Hakala, J., Hansel, A., Heinritzi, M., Hutterli, M., Kangasluoma, J., Kirkby, J., Laaksonen, A., Lehtipalo, K., Leiminger, M., Makhmutov, V., Mathot, S., Onnela, A., Petäjä, T., Praplan, A. P., Riccobono, F., Rissanen, M. P., Rondo, L., Schobesberger, S., Seinfeld, J. H., Steiner, G., Tomé, A., Tröstl, J., Winkler, P. M., Williamson, C., Wimmer, D., Ye, P., Baltensperger, U., Carslaw, K. S., Kulmala, M., Worsnop, D. R. and Curtius, J.: Neutral molecular cluster formation of sulfuric acid–dimethylamine observed in real time under atmospheric conditions, Proc. Natl. Acad. Sci., 111(42), 15019–15024, doi:10.1073/pnas.1404853111, 2014.

Kürten, A., Münch, S., Rondo, L., Bianchi, F., Duplissy, J., Jokinen, T., Junninen, H., Sarnela, N., Schobesberger, S., Simon, M., Sipilä, M., Almeida, J., Amorim, A., Dommen, J., Donahue, N. M., Dunne, E. M., Flagan, R. C., Franchin, A., Kirkby, J., Kupc, A., Makhmutov, V., Petäjä, T., Praplan, A. P., Riccobono, F., Steiner, G., Tomé, A., Tsagkogeorgas, G., Wagner, P. E., Wimmer, D., Baltensperger, U., Kulmala, M., Worsnop, D. R. and Curtius, J.: Thermodynamics of the formation of sulfuric acid dimers in the binary (H2SO4-H2O) and ternary (H2SO4-H2O-NH3) system, Atmos. Chem. Phys., 15(18), 10701–10721, doi:10.5194/acp-15-10701-2015, 2015.

Kürten, A., Bergen, A., Heinritzi, M., Leiminger, M., Lorenz, V., Piel, F., Simon, M., Sitals, R., Wagner, A. C. and Curtius, J.: Observation of new particle formation and measurement of sulphuric acid, ammonia, amines and highly oxidized organic molecules at a rural site in central Germany, Atmos. Chem. Phys., 16(19), 12793–12813, doi:10.5194/acp-16-12793-2016, 2016.

Kürten, A., Li, C., Bianchi, F., Curtius, J., Dias, A., Donahue, N. M., Duplissy, J., Flagan, R. C., Hakala, J., Jokinen, T., Kirkby, J., Kulmala, M., Laaksonen, A., Lehtipalo, K., Makhmutov, V., Onnela, A., Rissanen, M. P., Simon, M., Sipilä, M., Stozhkov, Y., Tröstl, J., Ye, P. and McMurry, P. H.: New particle formation in the sulfuric acid-dimethylamine-water system: Reevaluation of CLOUD chamber measurements and comparison to an aerosol nucleation and growth model, Atmos. Chem. Phys., 18(2), 845–863, doi:10.5194/acp-18-845-2018, 2018.

Kurtén, T., Noppel, M., Vehkamäki, H., Salonen, M. and Kulmala, M.: Quantum chemical studies of hydrate formation of H2SO4 and HSO4-, Boreal Environ. Res., 12(3), 431–453, 2007.

Kurtén, T., Loukonen, V., Vehkaméki, H. and Kulmala, M.: Amines are likely to enhance neutral and ion-induced sulphuric acid-water nucleation in the atmosphere more effectively than ammonia, Atmos. Chem. Phys., 8(14), 4095–4103, doi:10.5194/acp-8-4095-2008, 2008.

Lee, S. H., Gordon, H., Yu, H., Lehtipalo, K., Haley, R., Li, Y. and Zhang, R.: New Particle Formation in the Atmosphere: From Molecular Clusters to Global Climate, J. Geophys. Res. Atmos., doi:10.1029/2018JD029356, 2019.

Lehtinen, K. E. J., Dal Maso, M., Kulmala, M. and Kerminen, V. M.: Estimating nucleation rates from apparent particle formation rates and vice versa: Revised formulation of the Kerminen-Kulmala equation, J. Aerosol Sci., 38(9), 988–994, doi:10.1016/j.jaerosci.2007.06.009, 2007.

Lehtipalo, K., Yan, C., Dada, L., Bianchi, F., Xiao, M., Wagner, R., Stolzenburg, D., Ahonen, L. R., Amorim, A., Baccarini, A., Bauer, P. S., Baumgartner, B., Bergen, A., Bernhammer, A.-K., Breitenlechner, M., Brilke, S., Buchholz, A., Mazon, S. B., Chen, D., Chen, X., Dias, A., Dommen, J., Draper, D. C., Duplissy, J., Ehn, M., Finkenzeller, H., Fischer, L., Frege, C., Fuchs, C., Garmash, O., Gordon, H., Hakala, J., He, X., Heikkinen, L., Heinritzi, M., Helm, J. C., Hofbauer, V., Hoyle, C. R., Jokinen, T., Kangasluoma, J., Kerminen, V.-M., Kim, C., Kirkby, J., Kontkanen, J., Kürten, A., Lawler, M. J., Mai, H., Mathot, S., Mauldin, R. L., Molteni, U., Nichman, L., Nie, W., Nieminen, T., Ojdanic, A., Onnela, A., Passananti, M., Petäjä, T., Piel, F., Pospisilova, V., Quéléver, L. L. J., Rissanen, M. P., Rose, C., Sarnela, N., Schallhart, S., Schuchmann, S., Sengupta, K., Simon, M., Sipilä, M., Tauber, C., Tomé, A., Tröstl, J., Väisänen, O., Vogel, A. L., Volkamer, R., Wagner, A. C., Wang, M., Weitz, L., Wimmer, D., Ye, P., Ylisirniö, A., Zha, Q., Carslaw, K. S., Curtius, J., Donahue, N. M., Flagan, R. C., Hansel, A., Riipinen, I., Virtanen, A., Winkler, P. M., Baltensperger, U., Kulmala, M. and Worsnop, D. R.: Multicomponent new particle formation from sulphuric acid, ammonia, and biogenic vapors, Sci. Adv., 4(12), eaau5363, doi:10.1126/sciadv.aau5363, 2018.

Massoli, P., Stark, H., Canagaratna, M. R., Krechmer, J. E., Xu, L., Ng, N. L., Mauldin, R. L., Yan, C., Kimmel, J., Misztal, P. K., Jimenez, J. L., Jayne, J. T. and Worsnop, D. R.: Ambient Measurements of Highly Oxidized Gas-Phase Molecules during the Southern Oxidant and Aerosol Study (SOAS) 2013, ACS Earth Sp. Chem., 2(7), 653–672, doi:10.1021/acsearthspacechem.8b00028, 2018.

Mikkonen, S., Romakkaniemi, S., Smith, J. N., Korhonen, H., Petäjä, T., Plass-Duelmer, C., Boy, M., McMurry, P. H., Lehtinen, K. E. J., Joutsensaari, J., Hamed, A., Mauldin, R. L., Birmili, W., Spindler, G., Arnold, F., Kulmala, M. and Laaksonen, A.: A statistical proxy for sulphuric acid concentration, Atmos. Chem. Phys., 11(21), 11319–11334, doi:10.5194/acp-11-11319-2011, 2011.

Millán, M.: Extreme hydrometeorological events and climate change predictions in Europe, J. Hydrol., 518(PB), 206–224, doi:10.1016/j.jhydrol.2013.12.041, 2014.

Miller, M. R., Raftis, J. B., Langrish, J. P., McLean, S. G., Samutrtai, P., Connell, S. P., Wilson, S., Vesey, A. T., Fokkens, P. H. B., Boere, A. J. F., Krystek, P., Campbell, C. J., Hadoke, P. W. F., Donaldson, K., Cassee, F. R., Newby, D. E., Duffin, R. and Mills, N. L.: Inhaled Nanoparticles Accumulate at Sites of Vascular Disease, ACS Nano, 11(5), 4542–4552, doi:10.1021/acsnano.6b08551, 2017.

Minguillón, M. C., Brines, M., Pérez, N., Reche, C., Pandol, M., Fonseca, A. S., Amato, F., Alastuey, A., Lyasota, A., Codina, B., Lee, H., Eun, H., Ahn, K. and Querol, X.: New particle formation at ground level and in the vertical column over the Barcelona area, , 165, 118–130, doi:10.1016/j.atmosres.2015.05.003, 2015.

Minguillón, M.C., Pérez, N., Marchand, N., Bertrand, A., Temime-Roussel, B., Agrios, K., Szidat, S., van Drooge, B.L., Sylvestre, A., Alastuey, A., Reche, C., Ripoll, A., Marco, E., Grimalt, J.O., Querol, X.: Secondary organic aerosol origin in an urban environment. Influence of biogenic and fuel combustion precursors. Faraday Discuss., 189, 337-359, 2016.

Mohr, C., Thornton, J. A., Heitto, A., Lopez-Hilfiker, F. D., Lutz, A., Riipinen, I., Hong, J., Donahue, N. M., Hallquist, M., Petäjä, T., Kulmala, M. and Yli-Juuti, T.: Molecular identification of organic vapors driving atmospheric nanoparticle growth, Nat. Commun., 10(1), 1–7, doi:10.1038/s41467-019-12473-2, 2019.

Møller, K. H., Tram, C. M. and Kjaergaard, H. G.: Side-by-Side Comparison of Hydroperoxide and Corresponding Alcohol as Hydrogen-Bond Donors, J. Phys. Chem. A, 121(15), 2951–2959, doi:10.1021/acs.jpca.7b01323, 2017.

Molteni, U., Bianchi, F., Klein, F., El Haddad, I., Frege, C., Rossi, M. J., Dommen, J. and Baltensperger, U.: Formation of highly oxygenated organic molecules from aromatic compounds, Atmos. Chem. Phys., 18(3), 1909–1921, doi:10.5194/acp-18-1909-2018, 2018.

Ng, N. L., Herndon, S. C., Trimborn, A., Canagaratna, M. R., Croteau, P. L., Onasch, T. B., Sueper, D., Worsnop, D. R., Zhang, Q., Sun, Y. L. and Jayne, J. T.: An Aerosol Chemical Speciation Monitor (ACSM) for routine monitoring of the composition and mass concentrations of ambient aerosol, Aerosol Sci. Technol., 45(7), 770–784, doi:10.1080/02786826.2011.560211, 2011.

Olenius, T., Halonen, R., Kurtén, T., Henschel, H., Kupiainen-Määttä, O., Ortega, I. K., Jen, C. N., Vehkamäki, H. and Riipinen, I.: New particle formation from sulfuric acid and amines: Comparison of monomethylamine, dimethylamine, and trimethylamine, J. Geophys. Res., 122(13), 7103–7118, doi:10.1002/2017JD026501, 2017.

Olin, M., Kuuluvainen, H., Aurela, M., Kalliokoski, J., Kuittinen, N., Isotalo, M., Timonen, H. J., Niemi, J. V., Rönkkö, T., and Dal Maso, M.: Traffic-originated nanocluster emission exceeds H2SO4-driven photochemical new particle formation in an urban area, Atmos. Chem. Phys., 20, 1–13, https://doi.org/10.5194/acp-20-1-2020, 2020.

Ortega, I. K., Olenius, T., Kupiainen-Määttä, O., Loukonen, V., Kurtén, T., and Vehkamäki, H.: Electrical charging changes the composition of sulfuric acid–ammonia/dimethylamine clusters, Atmos. Chem. Phys., 14, 7995–8007, https://doi.org/10.5194/acp-14-7995-2014, 2014.

Paasonen, P., Olenius, T., Kupiainen, O., Kurtén, T., Petäjä, T., Birmili, W., Hamed, A., Hu, M., Huey, L. G., Plass-Duelmer, C., Smith, J. N., Wiedensohler, A., Loukonen, V., McGrath, M. J., Ortega, I. K., Laaksonen, A., Vehkamäki, H. and Kulmala, M.: On the formation of sulphuric acid – Amine clusters in varying atmospheric conditions and its influence on atmospheric new particle formation, Atmos. Chem. Phys., 12(19), 9113–9133, doi:10.5194/acp-12-9113-2012, 2012.

Pandolfi, M., Amato, F., Reche, C., Alastuey, A., Otjes, R. P., Blom, M. J. and Querol, X.: Summer ammonia measurements in a densely populated Mediterranean city, Atmos. Chem. Phys., 12(16), 7557–7575, doi:10.5194/acp-12-7557-2012, 2012.

Passananti, M., Zapadinsky, E., Zanca, T., Kangasluoma, J., Myllys, N., Rissanen, M. P., Kurtén, T., Ehn, M., Attoui, M. and Vehkamäki, H.: How well can we predict cluster fragmentation inside a mass spectrometer?, Chem. Commun., 55(42), 5946–5949, doi:10.1039/c9cc02896j, 2019.

Penner, J. E., Xu, L. and Wang, M.: Satellite methods underestimate indirect climate forcing by aerosols., Proc. Natl. Acad. Sci. U. S. A., 108(33), 13404–13408, doi:10.1073/pnas.1018526108, 2011.

Praske, E., Otkjær, R. V., Crounse, J. D., Hethcox, J. C., Stoltz, B. M., Kjaergaard, H. G. and Wennberg, P. O.: Atmospheric autoxidation is increasingly important in urban and suburban North America, Proc. Natl. Acad. Sci., 115(1), 64–69, doi:10.1073/pnas.1715540115, 2018.

Quéléver, L. L. J., Kristensen, K., Normann Jensen, L., Rosati, B., Teiwes, R., Daellenbach, K. R., Peräkylä, O., Roldin, P., Bossi, R., Pedersen, H. B., Glasius, M., Bilde, M. and Ehn, M.: Effect of temperature on the formation of highly oxygenated organic molecules (HOMs) from alpha-pinene ozonolysis, Atmos. Chem. Phys, 19, 7609–7625, doi:10.5194/acp-19-7609-2019, 2019.
Querol, X., Gangoiti, G., Mantilla, E., Alastuey, A., Minguillón, M. C., Amato, F., Reche, C., Viana, M., Moreno, T., Karanasiou, A., Rivas, I., Pérez, N., Ripoll, A., Brines, M., Ealo, M., Pandolfi, M., Lee, H. K., Eun, H. R., Park, Y. H., Escudero, M., Beddows, D., Harrison, R. M., Bertrand, A., Marchand, N., Lyasota, A., Codina, B., Olid, M., Udina, M., Jiménez-Esteve, B., Jiménez-Esteve, B. B., Alonso, L., Millán, M. and Ahn, K. H.: Phenomenology of high-ozone episodes in NE Spain, Atmos. Chem. Phys., 17(4), 2817–2838, doi:10.5194/acp-17-2817-2017, 2017.

Reche, C., Viana, M., Karanasiou, A., Cusack, M., Alastuey, A., Artiñano, B., Revuelta, M. A., López-Mahía, P., Blanco-Heras, G., Rodríguez, S., Sánchez de la Campa, A. M., Fernández-Camacho, R., González-Castanedo, Y., Mantilla, E., Tang, Y. S. and Querol, X.: Urban NH3 levels and sources in six major Spanish cities, Chemosphere, 119, 769–777, doi:10.1016/j.chemosphere.2014.07.097, 2015.

Riccobono, F., Schobesberger, S., Scott, C., Dommen, J., Ortega, I., Rondo, L., Almeida, J., Amorim, A., Bianchi, F., Breitenlechner, M., David, A., Downard, A., Dunne, E., Duplissy, J., Ehrhart, S., Flagan, R., Franchin, A., Hansel, A., Junninen, H., Kajos, M., Keskinen, H., Kupc, A., Kürten, A., Kvashin, A., Laaksonen, A., Lehtipalo, K., Makhmutov, V., Mathot, S., Nieminen, T., Onnela, A., Petäjä, T., Praplan, A., Santos, F., Schallhart, S., Seinfeld, J., Sipilä, M., Van Spracklen, D., Stozhkov, Y., Stratmann, F., Tomé, A., Tsagkogeorgas, G., Vaattovaara, P., Viisanen, Y., Vrtala, A., Wagner, P., Weingartner, E., Wex, H., Wimmer, D., Carslaw, K., Curtius, J., Donahue, N., Kirkby, J., Kulmala, M., Worsnop, D. and Baltensperger, U.: Oxidation products of biogenic emissions contribute to nucleation of atmospheric particles., Science (80-.)., 344(6185), 717–721, doi:10.1126/science.1243527, 2014.

Rissanen, M. P.: NO2 Suppression of Autoxidation-Inhibition of Gas-Phase Highly Oxidized Dimer Product Formation, ACS Earth Sp. Chem., 2(11), 1211–1219, doi:10.1021/acsearthspacechem.8b00123, 2018.

Rose, C., Zha, Q., Dada, L., Yan, C., Lehtipalo, K., Junninen, H., Mazon, S. B., Jokinen, T., Sarnela, N., Sipilä, M., Petäjä, T., Kerminen, V.-M., Bianchi, F. and Kulmala, M.: Observations of biogenic ion-induced cluster formation in the atmosphere, Sci. Adv., 4(4), 5218, doi:10.1126/sciadv.aar5218, 2018.

Schervish, M. and Donahue, N. M.: Peroxy radical chemistry and the volatility basis set, Atmos. Chem. Phys., 20(2), 1183–1199, doi:10.5194/acp-20-1183-2020, 2020.

Schobesberger, S., Junninen, H., Bianchi, F., Lönn, G., Ehn, M., Lehtipalo, K., Dommen, J., Ehrhart, S., Ortega, I. K., Franchin, A., Nieminen, T., Riccobono, F., Hutterli, M., Duplissy, J., Almeida, J., Amorim, A., Breitenlechner, M., Downard, A. J., Dunne, E. M., Flagan, R. C., Kajos, M., Keskinen, H., Kirkby, J., Kupc, A., Kürten, A., Kurtén, T., Laaksonen, A., Mathot, S., Onnela, A., Praplan, A. P., Rondo, L., Santos, F. D., Schallhart, S., Schnitzhofer, R., Sipilä, M., Tomé, A., Tsagkogeorgas, G., Vehkamäki, H., Wimmer, D., Baltensperger, U., Carslaw, K. S., Curtius, J., Hansel, A., Petäjä, T., Kulmala, M., Donahue, N. M. and Worsnop, D. R.: Molecular understanding of atmospheric particle formation from sulphuric acid and large oxidized organic molecules., Proc. Natl. Acad. Sci. U. S. A., 110(43), 17223–17228, doi:10.1073/pnas.1306973110, 2013.

Simon, M., Heinritzi, M., Herzog, S., Leiminger, M., Bianchi, F., Praplan, A., Dommen, J., Curtius, J. and Kurten, A.: Detection of dimethylamine in the low pptv range using nitrate chemical ionization atmospheric pressure interface time-of-flight (CI-APi-TOF) mass spectrometry, Atmos. Meas. Tech., 9(5), 2135–2145, doi:10.5194/amt-9-2135-2016, 2016.

Sipilä, M., Sarnela, N., Jokinen, T., Henschel, H., Junninen, H., Kontkanen, J., Richters, S., Kangasluoma, J., Franchin, A., Peräkylä, O., Rissanen, M. P., Ehn, M., Vehkamäki, H., Kurten, T., Berndt, T., Petäjä, T., Worsnop, D., Ceburnis, D., Kerminen, V. M., Kulmala, M. and O'Dowd, C.: Molecular-scale evidence of aerosol particle formation via sequential addition of HIO3, Nature, 537(7621), 532–534, doi:10.1038/nature19314, 2016.

Stolzenburg, D., Fischer, L., Vogel, A. L., Heinritzi, M., Schervish, M., Simon, M., Wagner, A. C., Dada, L., Ahonen, L. R., Amorim, A., Baccarini, A., Bauer, P. S., Baumgartner, B., Bergen, A., Bianchi, F., Breitenlechner, M., Brilke, S., Buenrostro Mazon, S., Chen, D., Dias, A., Draper, D. C., Duplissy, J., El Haddad, I., Finkenzeller, H., Frege, C., Fuchs, C., Garmash, O., Gordon, H., He, X., Helm, J., Hofbauer, V., Hoyle, C. R., Kim, C., Kirkby, J., Kontkanen, J., Kürten, A., Lampilahti, J., Lawler, M., Lehtipalo, K., Leiminger, M., Mai, H., Mathot, S., Mentler, B., Molteni, U., Nie, W., Nieminen, T., Nowak, J. B., Ojdanic, A., Onnela, A., Passananti, M., Petäjä, T., Quéléver, L. L. J., Rissanen, M. P., Sarnela, N., Schallhart, S., Tauber, C., Tomé, A., Wagner, R., Wang, M., Weitz, L., Wimmer, D., Xiao, M., Yan, C., Ye, P., Zha, Q., Baltensperger, U., Curtius, J., Dommen, J., Flagan, R. C., Kulmala, M., Smith, J. N., Worsnop, D. R., Hansel, A., Donahue, N. M. and Winkler, P. M.: Rapid growth of organic aerosol nanoparticles over a wide tropospheric temperature range, Proc. Natl. Acad. Sci., 201807604 [online] Available from: http://www.pnas.org/lookup/doi/10.1073/pnas.1807604115, 2018.

Tröstl, J., Chuang, W. K., Gordon, H., Heinritzi, M., Yan, C., Molteni, U., Ahlm, L., Frege, C., Bianchi, F., Wagner, R., Simon, M., Lehtipalo, K., Williamson, C., Craven, J. S., Duplissy, J., Adamov, A., Almeida, J., Bernhammer, A. K., Breitenlechner, M., Brilke, S., Dias, A., Ehrhart, S., Flagan, R. C., Franchin, A., Fuchs, C., Guida, R., Gysel, M., Hansel, A., Hoyle, C. R., Jokinen, T., Junninen, H., Kangasluoma, J., Keskinen, H., Kim, J., Krapf, M., Kürten, A., Laaksonen, A., Lawler, M., Leiminger, M., Mathot, S., Möhler, O., Nieminen, T., Onnela, A., Petäjä, T., Piel, F. M., Miettinen, P., Rissanen, M. P., Rondo, L., Sarnela, N., Schobesberger, S., Sengupta, K., Sipilä, M., Smith, J. N., Steiner, G., Tomè, A., Virtanen, A., Wagner, A. C., Weingartner, E., Wimmer, D., Winkler, P. M., Ye, P., Carslaw, K. S., Curtius, J., Dommen, J., Kirkby, J., Kulmala, M., Riipinen, I., Worsnop, D. R., Donahue, N. M. and Baltensperger, U.: The role of low-volatility organic compounds in initial particle growth in the atmosphere, Nature, 533(7604), 527–531, doi:10.1038/nature18271, 2016.

Van Damme, M., Clarisse, L., Whitburn, S., Hadji-Lazaro, J., Hurtmans, D., Clerbaux, C. and Coheur, P. F.: Industrial and agricultural ammonia point sources exposed, Nature, 564(7734), 99–103, doi:10.1038/s41586-018-0747-1, 2018.

Wang, S., Wu, R., Berndt, T., Ehn, M. and Wang, L.: Formation of Highly Oxidized Radicals and Multifunctional Products from the Atmospheric Oxidation of Alkylbenzenes, Environ. Sci. Technol., 51(15), 8442–8449, doi:10.1021/acs.est.7b02374, 2017.

Yan, C.: The role of H2SO4-NH3 anion clusters in ion-induced aerosol nucleation mechanisms in the boreal forest, Atmos. Chem. Phys., (April), 1–20, doi:10.1029/2001JD001100, 2018.

Yan, C., Nie, W., Äijälä, M., Rissanen, M. P., Canagaratna, M. R., Massoli, P., Junninen, H., Jokinen, T., Sarnela, N., Häme, S. A. K., Schobesberger, S., Canonaco, F., Yao, L., Prévôt, A. S. H., Petäjä, T., Kulmala, M., Sipilä, M., Worsnop, D. R. and Ehn, M.: Source characterization of highly oxidized multifunctional compounds in a boreal forest environment using positive matrix factorization, Atmos. Chem. Phys., 16(19), 12715–12731, doi:10.5194/acp-16-12715-2016, 2016.

Yan, C., Nie, W., Vogel, A. L., Dada, L., Lehtipalo, K., Stolzenburg, D., Wagner, R., Rissanen, M. P., Xiao, M., Ahonen, L., Fischer, L., Rose, C., Bianchi, F., Gordon, H., Simon, M., Heinritzi, M., Garmash, O., Roldin, P., Dias, A., Ye, P., Hofbauer, V., Amorim, A., Bauer, P. S., Bergen, A., Bernhammer, A.-K., Breitenlechner, M., Brilke, S., Buchholz, A., Mazon, S. B., Canagaratna, M. R., Chen, X., Ding, A., Dommen, J., Draper, D. C., Duplissy, J., Frege, C., Heyn, C., Guida, R., Hakala, J., Heikkinen, L., Hoyle, C. R., Jokinen, T., Kangasluoma, J., Kirkby, J., Kontkanen, J., Kürten, A., Lawler, M. J., Mai, H., Mathot, S., Mauldin, R. L., Molteni, U., Nichman, L., Nieminen, T., Nowak, J., Ojdanic, A., Onnela, A., Pajunoja, A., Petäjä, T., Piel, F., Quéléver, L. L. J., Sarnela, N., Schallhart, S., Sengupta, K., Sipilä, M., Tomé, A., Tröstl, J., Väisänen, O., Wagner, A. C., Ylisirniö, A., Zha, Q., Baltensperger, U., Carslaw, K. S., Curtius, J., Flagan, R. C., Hansel, A., Riipinen, I., Smith, J. N., Virtanen, A., Winkler, P. M., Donahue, N. M., Kerminen, V.-M., Kulmala, M., Ehn, M. and Worsnop, D. R.: Size-dependent influence of NOx on the growth rates of organic aerosol particles , Sci. Adv., 6(22), eaay4945, doi:10.1126/sciadv.aay4945, 2020.

Yao, L., Garmash, O., Bianchi, F., Zheng, J., Yan, C., Kontkanen, J., Junninen, H., Mazon, S. B., Ehn, M., Paasonen, P., Sipilä, M., Wang, M., Wang, X., Xiao, S., Chen, H., Lu, Y., Zhang, B., Wang, D., Fu, Q., Geng, F., Li, L., Wang, H., Qiao, L., Yang, X., Chen, J., Kerminen, V. M., Petäjä, T., Worsnop, D. R., Kulmala, M. and Wang, L.: Atmospheric new particle formation from sulphuric acid and amines in a Chinese megacity, Science (80-.)., 361(6399), 278–281, doi:10.1126/science.aao4839, 2018.

Yli-Juuti, T., Pajunoja, A., Tikkanen, O. P., Buchholz, A., Faiola, C., Väisänen, O., Hao, L., Kari, E., Peräkylä, O., Garmash, O., Shiraiwa, M., Ehn, M., Lehtinen, K. and Virtanen, A.: Factors controlling the evaporation of secondary organic aerosol from α-pinene ozonolysis, Geophys. Res. Lett., 44(5), 2562–2570, doi:10.1002/2016GL072364, 2017.

Yu, H., Zhou, L., Dai, L., Shen, W., Dai, W., Zheng, J., Ma, Y. and Chen, M.: Nucleation and growth of sub-3 nm particles in the polluted urban atmosphere of a megacity in China, Atmos. Chem. Phys., 16(4), 2641–2657, doi:10.5194/acp-16-2641-2016, 2016.

Zhang, R., Khalizov, A., Wang, L., Hu, M. and Xu, W.: Nucleation and growth of nanoparticles in the atmosphere, Chem. Rev., 112(3), 1957–2011, doi:10.1021/cr2001756, 2012.

Zhao, J., Eisele, F. L., Titcombe, M., Kuang, C. and McMurry, P. H.: Chemical ionization mass spectrometric measurements of atmospheric neutral clusters using the cluster-CIMS, J. Geophys. Res., 115(D8), 1–19, doi:10.1029/2009jd012606, 2010.

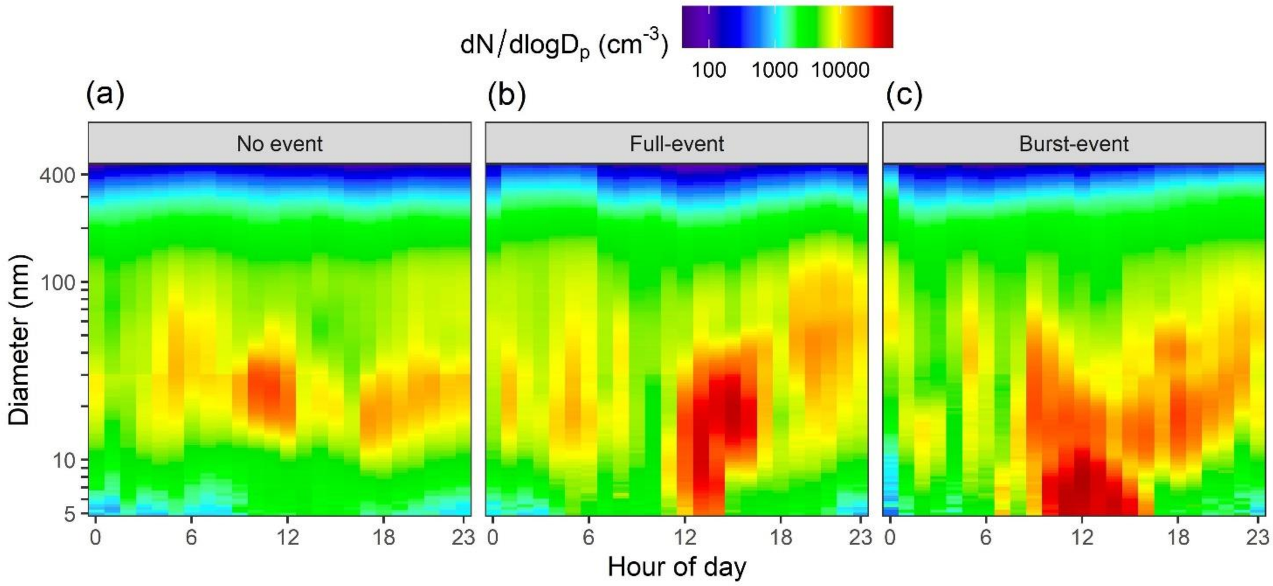

Figure 1: Average SMPS contour plots for (a) non-event days, (b) full-event days and (c) burst-event days.

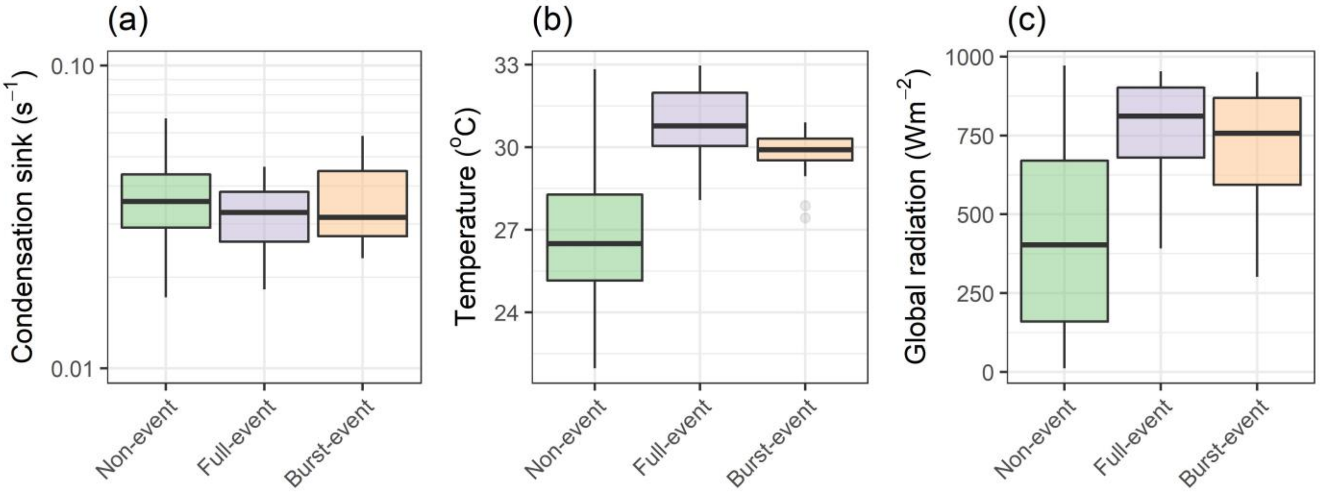

Figure 2: Box plots for days of non-event, full-event and burst-event, showing (a) condensation sink, (b) temperature, and (c) global radiation from hourly data. "Full-event" and "burst-event" include data across the entire day.

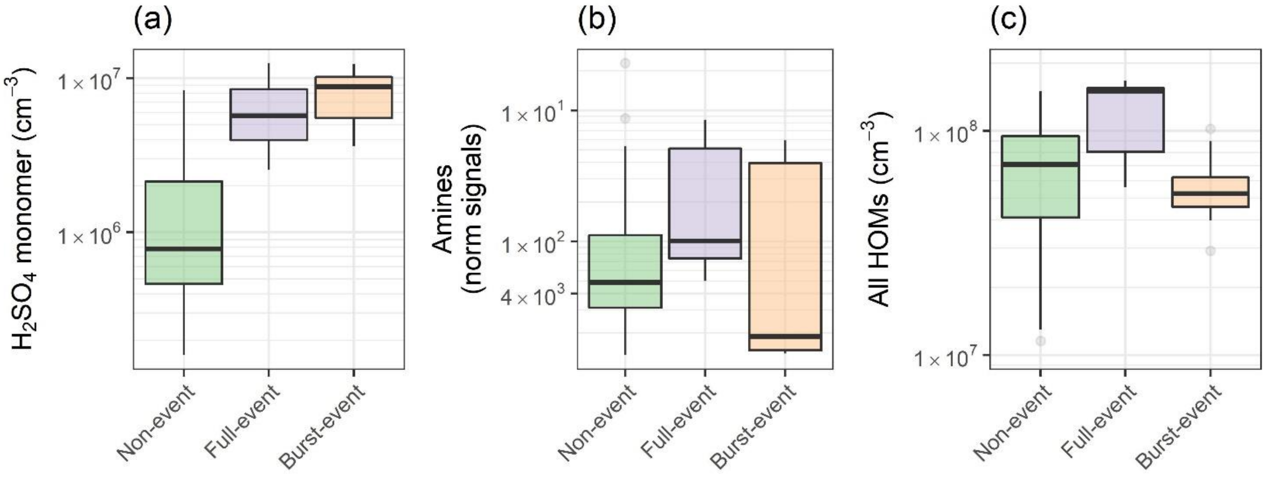

Figure 3: Box plots for days of non-event, full-event and burst-event, showing (a) sulphuric acid, (b) C_2 and C_4 amines, as clustered with the nitrate dimer and trimer, and (c) summed HOM concentration from C_5+ from hourly data. Units for ammonia + amines are normalised counts, as no calibration was performed. Event days include data across the full event day.

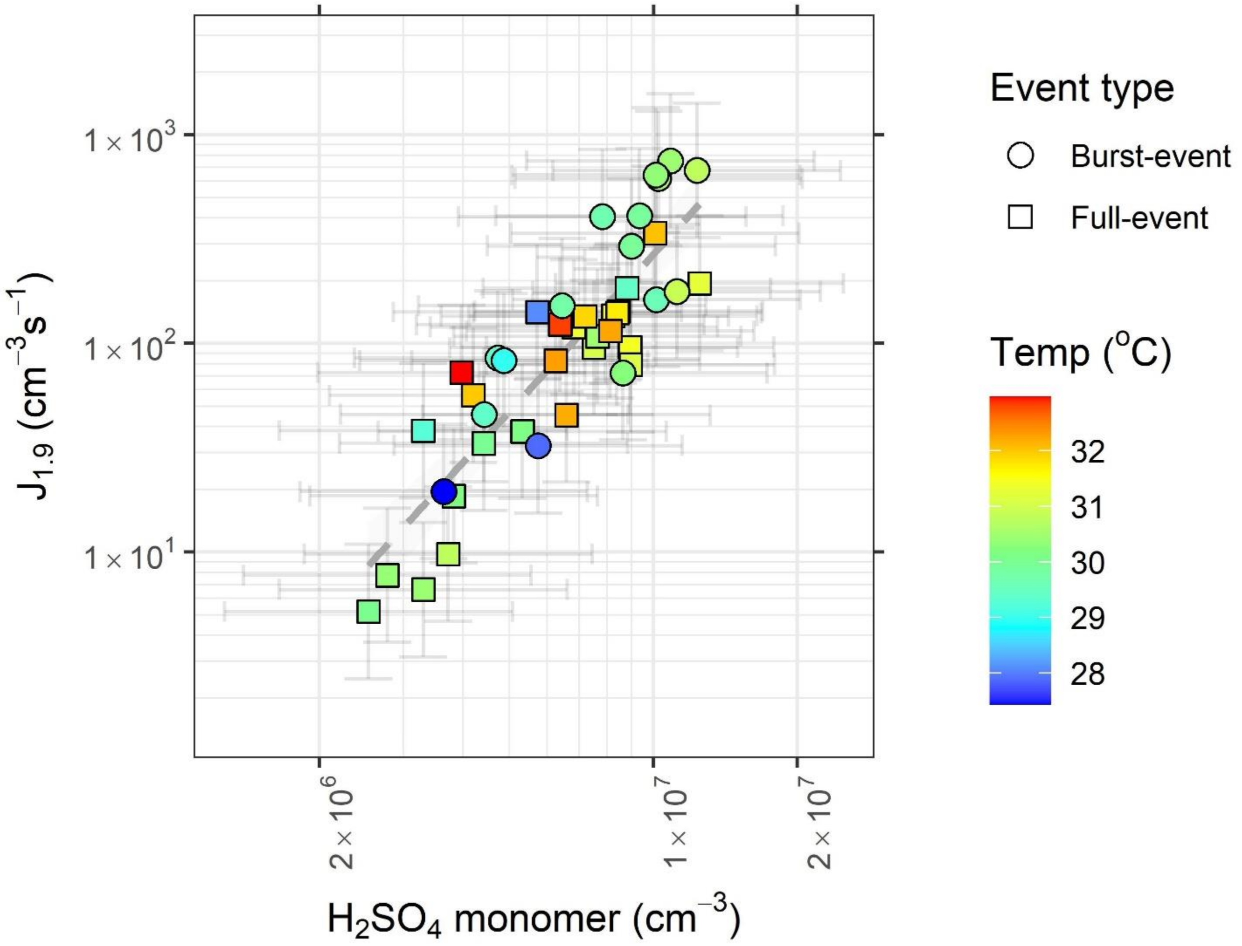

Figure 4: Formation rate ($J_{1.9}$) plotted against sulphuric acid monomer concentration, coloured by condensation sink. Circles represent burst-events, squares represent full events. Data is for hourly averages across NPF periods, typically within the hours 08:00 – 16:00. Slope of the line = $4.9 \cdot 10^{-5}$ s^{-1}. Error bars represent systematic uncertainties on [H_2SO4] and $J_{1.9}$

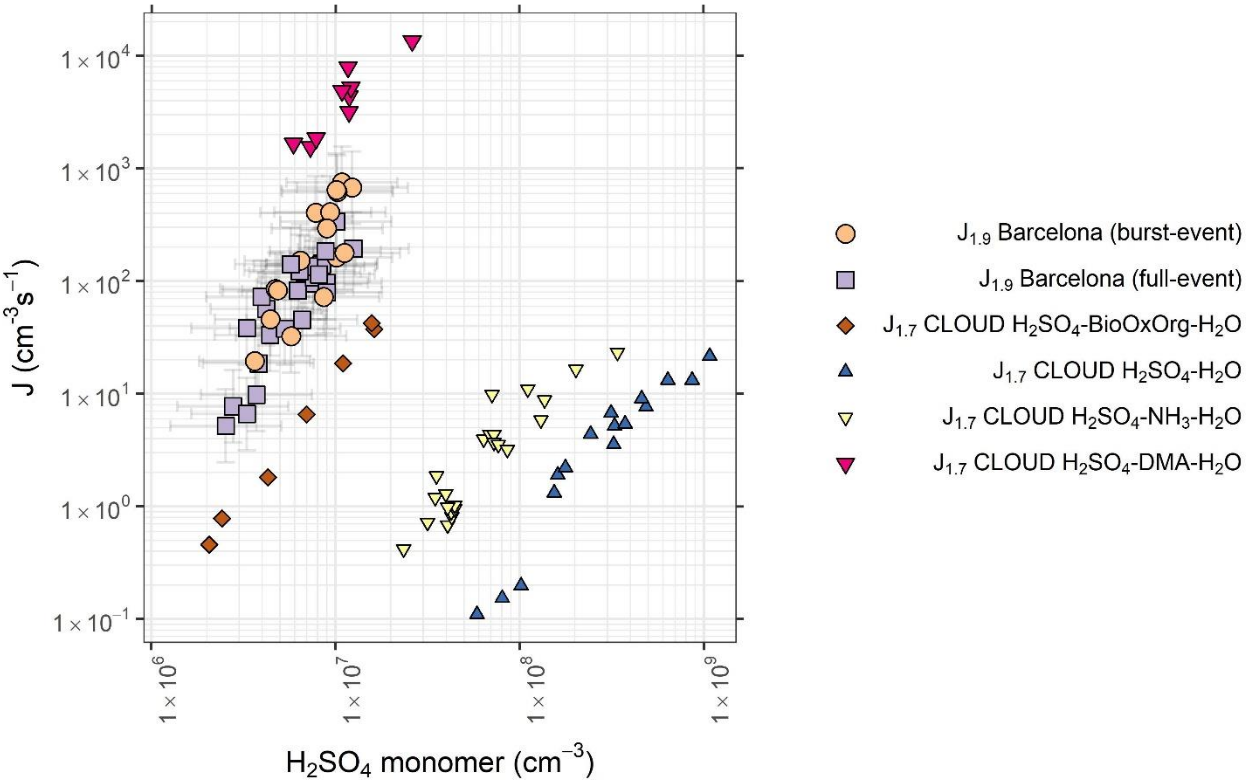

Figure 5: Formation rate plotted against sulphuric acid monomer concentration for data collected from Barcelona. Tan circles represent burst-events, purple squares represent full events. as well as that for the H_2SO_4-H_2O (blue inverted triangles), H_2SO_4-NH_3-H_2O (yellow inverted triangles), H_2SO_4-DMA-H_2O (pink triangles), and H_2SO_4-BioOxOrg-H_2O (brown diamonds) systems from the CLOUD chamber (Kürten et al., 2018 Kirkby et al., 2011; Riccobono et al., 2014). CLOUD chamber experiments were performed at 278 K and 38 – 39 % RH. Data is for hourly averages across NPF periods, typically within the hours 08:00 – 16:00. Error bars represent systematic uncertainties on [H_2SO_4] and $J_{1.9}$.

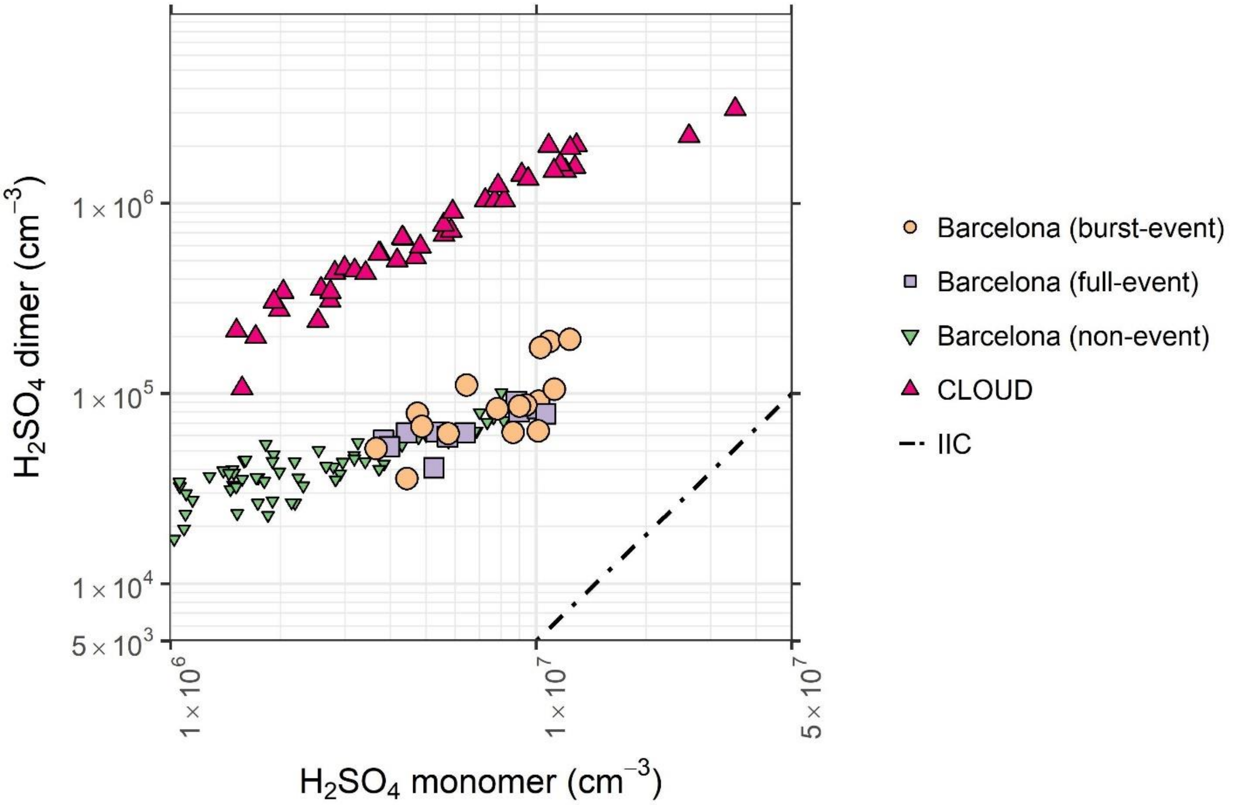

Figure 6: Sulphuric acid dimer concentration plotted against monomer concentration, showing burst-event periods (tan circles), full event periods (purple squares), non-event periods (green inverted triangles), and the ratio of sulphuric acid dimer:monomer in the CLOUD chamber for the H_2SO_4-H_2O-DMA system (pink triangles) (Almeida et al., 2013). Dashed line represents the dimer concentration produced by ion induced clustering in the chemical ionization unit (Zhao et al., 2010). CLOUD chamber experiments were performed at 278 K and 38 – 39 % RH. Data is for hourly averages across NPF periods, typically within the hours 08:00 – 16:00. Error bars represent systematic uncertainties on $[H_2SO_4]$ and $[(H_2SO_4)_2]$.

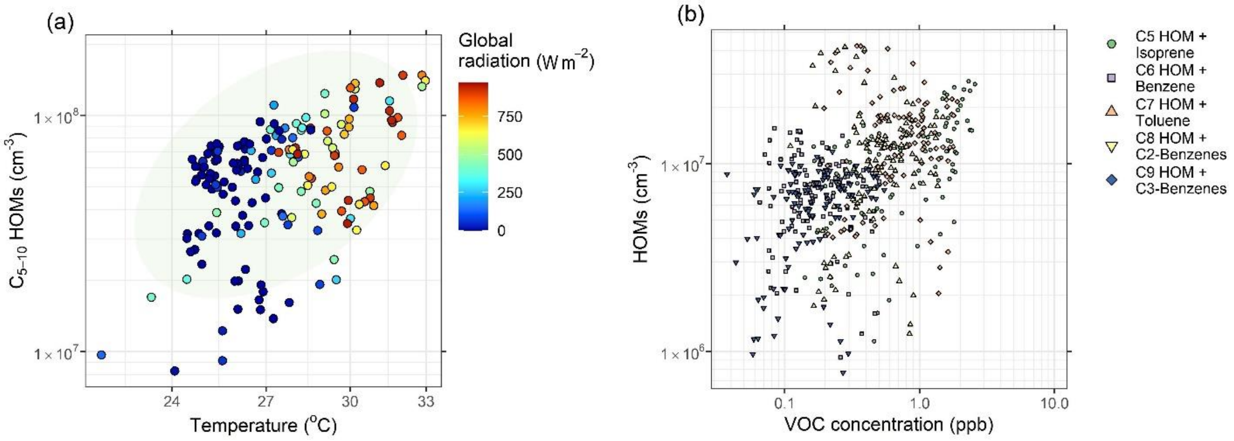

Figure 7: Influencing factors on HOM concentration, showing (a) C_{5-10} HOM concentration plotted against temperature, coloured by global radiation. Ellipsis shows 95% confidence on a multivariate t-distribution. (b)HOM concentration by carbon number potted against parent VOC mixing ratio. These are segregated by carbon number/VOC, i.e, C_7 HOMs plotted against toluene, under the assumption that toluene oxidation is the main producer of C_7 HOMs. Time for both plots is of hourly time resolution.

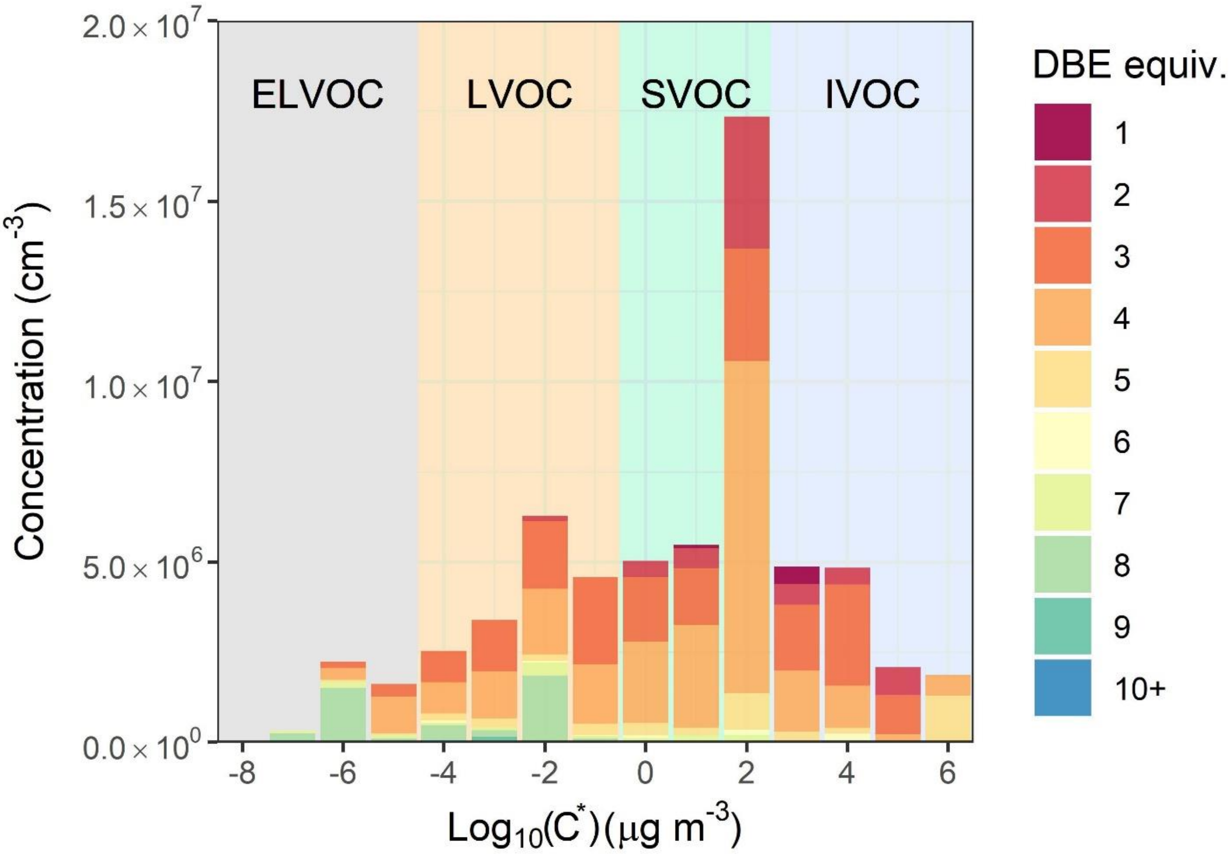

Figure 8: Concentrations of all oxygenated organic molecules and HOMs binned to integer $Log_{10}(C^*)$ values, coloured by DBE.

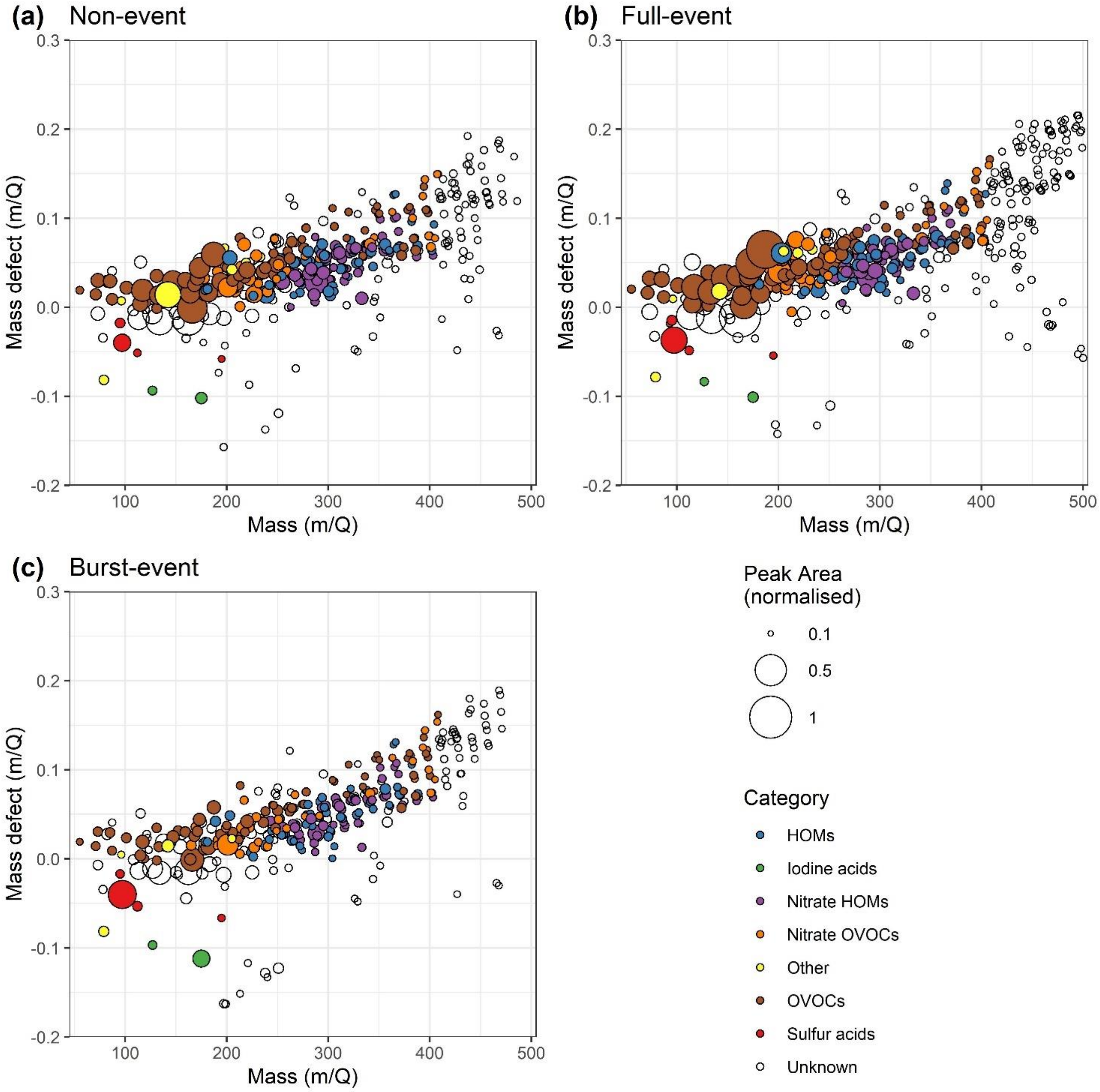

Figure 9: Mass defect plots for (a) non-event, (b) full-event, and (c) burst-event periods, data taken from 10:00 – 15:00 on the days 11/07/2018, 16/07/2018 and 15/07/2018 respectively. Size corresponds to mass spectral peak area. Ions are coloured according to identified chemical composition. *Blue* points correspond to HOMs containing all organic species with ≥5 carbon atoms and ≥6 oxygen atoms, and an O:C ratio of >0.6. *Purple* points correspond to the same but for species containing 1-2 nitrogen atoms. Species not meeting this HOM criterea were classed generally as OVOCs which are coloured *brown*, with the nitrogen containing OVOCs coloured *orange*. Sulphur acids (*red*) include ions HSO_4^-, $CH_3SO_3^-$ and SO_5^-, as well as the sulphuric acid dimer. Iodine acids (*green*) contains both IO_3^- and I^- (the latter presumably deprotonated hydrogen iodide). Unidentified points are left uncoloured.